CHAPTER III

RESULTS AND DISCUSSION

3.1 Synthesis of Macrocyclic and Open-chain Schiff-base Compounds

3.1.1 Preparation of Bis(salicylaldehyde)*N,N*′-ethylene diimine: Salen and Bis (salicylaldehyde)*N,N*′-tri methylenediimine: Saltn

The synthetic processes for Salen and Saltn were described as process I and II, respectively,in Scheme IV. The starting material for the preparation of Salen, salicylaldehyde, was introduced to react with ethylenediamine in ethanol which called "Schiff-base" reaction. The absence of water and cooling condition were nescessary. The pure Salen was obtained as bright yellow precipitate after recrystalization from warm acetone with a good yield. For Saltn, the process was similar to the preparation of Salen by using 1,3 diaminopropane instead of ethylenediamine and the desired product was obtained as greenish yellow precipitate. Methanol and/or ethanol could be used as solvent in this reaction and petroleum spirit,40-60 °c, was chosen as solvent for recrystallization. Particularly,warm acetone can not be used in this reaction because the solution be-

came oily after dissolving the greenish yellow product in acetone.

3.1.2 Preparation of 1,4 Bis (2′-formylphenyl)-1,4 -dioxabutane: O-en and 1,5- Bis(2′-formylphenyl) -1,5 dioxapentone: O-tn

Salicylaldehyde was also employed as starting material for preparation of both O-en and O-tn. Williamson condensation between salicylaldehyde and dibromoalkane was used in the present work to obtain dialdehyde : O-en and O-tn as III,V respectively in Scheme IV. The reaction time for O-en was a little longer than for O-tn. Dichloroalkane could also be used instead of dibromoalkane but reaction time to obtain the product was much longer and the the yield was lower than using dibromoalkane. This was due to the stronger Cl-C bond than Br-C bond. The presence of nitrogen flow was very important to protect oxidation from air during the reaction. The disappearance of the reactant and the formation of the products were monitored by TLC. After the reaction was completed, the solution was stirred on ice at 0 °c until the precipitate was produced then left stand at 0 °c in the refrigerator to produce more crystals. Both products (O-en and O-tn) were recrystallized from chloroform:ether (50:50)solvent.

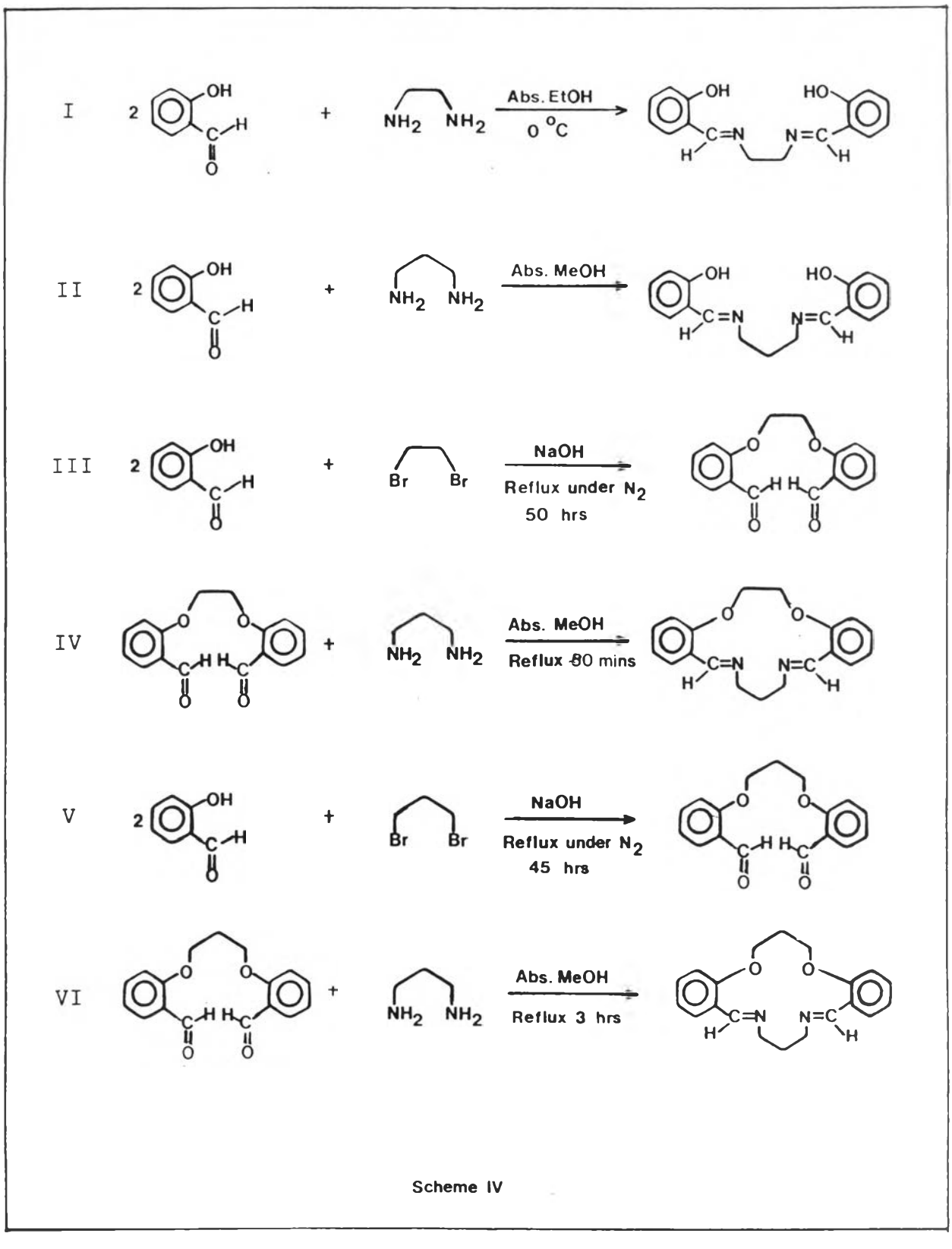
I
2
OH
C
H
O
+
NH2 NH2
Abs. EtOH
0 °C
OH
HO
C=N
N=C
H
H
II
2
OH
C
H
O
+
NH2 NH2
Abs. MeOH
OH
HO
C=N
N=C
H
H
III
2
OH
C
H
O
+
Br Br
NaOH
Reflux under N2
50 hrs
O
O
C H H C
O
O
IV
O
O
C H H C
O
O
+
NH2 NH2
Abs. MeOH
Reflux 30 mins
O
O
C=N
N=C
H
H
V
2
OH
C
H
O
+
Br Br
NaOH
Reflux under N2
45 hrs
O
O
C H H C
O
O
VI
O
O
C H H C
O
O
+
NH2 NH2
Abs. MeOH
Reflux 3 hrs
O
O
C=N
N=C
H
H

Scheme IV

3.1.3 Preparation of 3,4,9,10-Dibenzo-1,13 diaza-5,9 -dioxacyclohexadecane-1-12-diene : O-en-N-tn and 3,4,10,11-Dibenzo-1,13-diaza-5,9-dioxacyclo hexadecane-1-13-diene:O-tn-N-tn

O-en-N-tn and O-tn-N-tn were successfully synthesized by reacting 1,2-diaminopropane with corresponding dialdehyde in methanol as IV and VI in Scheme IV. The macrocyclic compounds can be isolated from the methanol reaction solution by the addition of water. O-en-N-tn was obtained with good yield (92.86 %) while the reaction yielding O-tn-N-tn gave a vary low yield (29.5%). This was propably due to the possibility of polymer formation. The other synthetic route to synthesize these macrocyclic Schiff-base compounds was also tried by first reacting the salicylaldehyde with diamine to obtain Saltn and then reacting Saltn with appropriate dihaloalkane to cyclize the ring but the last step of cyclization was unsuccessful.

Some physical properties of all synthetic compounds are listed in Table 3.1.

Table 3.1 Physical properties of the synthetic compounds

Compound	Color	mp (°c)	yield (%)
Salen	bright yellow	120-121	91.79
Saltn	greenish yellow	50-51	87.94
O-en	cream	123-124	44.80
O-tn	Spale cream	91-92	92.86
O-en-N-tn	white	149-150	59.80
O-tn-N-tn	white	155-157	29.50

3.2 Structural Elucidation of the Synthesized Schiff-base Compounds.

3.2.1 Infrared Spectroscopic Properties of Schiff-base Compounds

IR spectra of all compounds were obtained as KBr pellets as shown in Figures 3.1,3.5,3.9,3.13.3.17,and 3.21, and their main IR bands were listed in Tables 3.2. IR spectra of Salen and Saltn were essentially the same as shown in Figures 3.1 and 3.5 ,respectively. Of specific interest was the C=N stretching around 1640 cm^{-1} and O-H stretching around 2800 cm^{-1} which were observed to shift from normal O-H stretching (3200-3600 cm^{-1})due to formation of hydrogen bond between hydrogen atom from O-H group and nitrogen atom at C=N. IR spectra of O-en and O-tn,Figures 3.9 and 3.17 respectively,showed a very strong band at 1690 cm^{-1} of C=O stretching (carbonyl group) and a strong band at 1600 cm^{-1} of C=C stretching (aromatic mode). IR spectra of both macrocyclic Schift-base compounds (O-en-N-tn,Figure 3.13 and O-tn-N-tn,Figure 3.21 appeared to be similar to each other and each exhibited C=N stretching band at 1630 -1635 cm^{-1} which confirmed the Schiff-base condensation between O-en,O-tn and diamine. This was further confirmed by the absence of the carbonyl absorption band(1690 cm^{-1}).

3.2.2 Nuclear Magnetic Resonance Spectroscopic Properties of Schiff-base Compounds

Both proton and carbon-13 NMR spectra were studied for each compound synthesized in this work. The proton NMR spectra were able to characterize aliphatic and aromatic proton patterns while carbon-13 NMR spectra indicated the number of carbon atoms and their positions. $CDCl_3$ was used as solvent of choice for NMR study thoughout this work. The obtained ^1H and ^{13}C NMR spectra for all Schiff-base compounds,Figure 3.2,3.3,3.6,3.7,3.10,3.11,3.1,4,3.15,3.18 and 3.19, were assigned as detailed in Tables 3.3 and 3.4, respectively. These spectra were in accord with the proposed structures. ^1H NMR spectrum of Salen,Figure 3.2, was quite simple,due to the symmetrical structure. It consisted of peaks in three regions, one of which was a sharp signal occurring at 3.8 ppm due to the protons of methylene groups (CH_2). The second region, between 6.8 and 7.3 ppm,is characteristic of the aromatic protons. The signal at 8.3 ppm has been assigned to the imine protons (-HC=N-). The third signal at 13.2 ppm was due to phenolic protons and the broad appearence indicatede that it probably was involved in intramolecular hydrogen bonding (N···H···O)

^{13}C NMR spectrum of Salen as shown in Figure 3.4 has eight main peaks as listed in Table 3.4. ^{13}C NMR spectral data were also consistent with the proposed structure

for Salen. Figure 3.6 shows ^{1}H spectrum of Saltn,it was more complicated than that of Salen by an increment of the quintet peak at 1.9-2.1 ppm which indicated the presence of a methylene group in between two methylene groups ($-CH_2-CH_2-CH_2-$). Its ^{13}C NMR spectrum (Figure 3.7) confirmed the structure of Saltn by showing nine peaks in the spectrum at appropriate ppm's. NMR spectral studies of O-en and O-tn in $CDCl_3$ revealed in Figures 3.10 and 3.11 for O-en and Figures 3.18 and 3.19 for O-tn. O-en could be distinguishes from O-tn by a difference in number of carbon atoms in aliphatic chain which was also exhibited by an increment of the quintet signal of the methylene group at 2.3-2.5 ppm for O-tn. Other signals were assigned as detailed in Table 3.4. ^{1}H NMR and ^{13}C NMR spectra for the macrocyclic compound ; O-en-N-tn were exhibited in Figure 3.14 and Figure 3.15, respectively. Both ^{1}H and ^{13}C NMR spectra of O-en-N-tn show the expected pattern confirming the presence of imine, aromatic and methylene protons as detailed in Table 3.3 and 3.4. On the other hand, ^{1}H and ^{13}C spectra of O-tn-N-tn were a little more complex as also shown in figure 3.22 and 3.23 respectively.

3.2.3 Mass Spectrometry of Schiff-base Compounds

Mass spectral studies were also done to support the proposed structures for the synthesized compounds. The major features and the postulated fragment ions of each

spectrum were summarized in Table 3.5.

The mass spectrum of Salen, Figure 3.4, exhibited the molecular ion peak at m/e 268 and also shew the peak (M^++1) at m/e 269. In this case the molecular ion was the base peak. In addition,it shew ion corresponding to half the molecular ion (m/e 134), ions resulting from cleavage of nitrogen-carbon bond of the diamine (m/e 122) were also predominant. The other fragment ions were benzene ring character observed with high intensity. The mass spectrum of Saltn,Figure 3.8, shew its molecular ion peak at m/e 282 and the peak M^++1 at m/e 283. The other fragment ions are similar to those occured in Salen. The mass spectrum of O-en (Figure 4.12) shew a molecular ion peak at m/e 270,the base peak at m/e 121 and the other postulated fragment ions were tabulated in Table 3.5. In Figure 3.20 shew mass spectrum of O-tn , similar pattern to that of O-en was observed,that was molecular ion peak at m/e 284 and base peak appeared at m/e 121. The mass spectrum of O-en-N-tn was shown in Figure 3.16. Its molecular ion peak was observed at m/e 308 and the base peak appears at m/e 162. The other major peaks were exhibited in Table 3.5. The mass spectrum of O-tn-N-tn was shown in Figure 3.24. The molecular ion peak at m/e 322 was also illustrated to be the base peak. Due to the high symmetry of the synthesized compounds,all fragmentation patterns appear to be similar to their corresponding analogue. All compounds shown frag-

ment ions corresponding to benzene ring character such as m/e at 91,79,78,77,65,51,etc.

The fragmentation patterns follow a very straightforward form which was always compatible with cleavage of 2 or 3 carbon bridge and some fragment ions shew some rearrangments to more stable ions.

3.2.4 Elemental Analysis of Schiff-base Compounds

The elemental percentages of C,H and N were compared with their calculated values of synthetic compounds are listed in Table 3.6. All compounds shew excellent agreements of the values which supported the proposed formulas and structures for the synthesized compounds.

Table 3.2 Assignment of vibrational modes of the Schiff -base compounds

Compound	vibrational frequency (cm^{-1})	Intensity	assignment
Salen	3050-3010	w	C-H stretching (aromatic)
	2870,2900,2930,2950	w	C-H stretching (Alkyl gr.)
	2800	w	O-H stretching (broad)
	1640	m	C=N stretching (imine)
	1610,1580,1500	m	C-C stretching (aromatic)
	1450	s	C-H bending (CH_2 gr.)
	765,740	s	C-H out of plane (bending of aromatic)
Saltn	3060-3010	w	C-H stretching (aromatic)
	2860,2920,2940	w	C-H stretching (alkyl gr.)
	2730	w	O-H stretching (broad)
	1635	m	C=N stretching (imine)

Table 3.2 (continued)

Compound	vibrational frequency (cm^{-1})	Intensity	assignment
Saltn	1610,1580,1500	m	C-C stretching (aromatic)
	1450	s	C-H bending (CH_2 gr.)
	760,740	s	C-H out of plane(benting of (arometic)
O-en	3020-3100	w	C-H stretching (aromatic)
	2940,2860	s	C-H stretching (aliphatic)
	2760	m	C-H stretching (carbonyl gr)
	1690	vs	C=O stretching
	1600,1580,1480	s	C-C stretching (aromatic)
	1450	s	C-H bending (CH_2 gr.)
	1240	s	C-O-C stretching (asym)
	750	s	C-H bending out of plane

Table 3.2 (continued)

Compound	vibrational frequency (cm^{-1})	Intensity	assignment
O-tn	3020,3100	m	C-H stretching (aromatic)
	2860,2960,2900	s	C-H stretching (aliphatic)
	2760	m	C-H stretching (carbonyl gr)
	1690	s	C=O stretching
	1600,1500	s	C=C stretching (aromatic)
	1460	s	C-H bending (CH_2 gr.)
	1240	s	C-O-C stretching (asym)
	750	s	C-H out of plane (bending of aromatic)
O-en-N-tn	3030-3080	m	C-H stretching (aromatic)
	2820-2940	s	C-H stretching (aliphatic)
	1630	vs	-C=N-stretching
	1600,1485,1590	s	C-C stretching (aromatic)

Table 3.2 (continued)

Compound	vibrational frequency (cm^{-1})	Intensity	assignment
	1450	s	C-H bending (CH_2 gr.)
	1230	s	C-O-C stretching (asym)
	1030-1070	m	C-H in plane bending of aromatic
	750	s	C-H out of plane (bending of aromatic)
O-tn-N-tn	3015-3080	m	C-H stretching (aromatic)
	2840-2940	s	C-H stretching (aliphatic)
	1635	vs	C=N stretching
	1600,1580,1490	s	C-C stretching (aromatic)
	1455	s	C-H bending (CH_2 gr.)
	1235-1250	s	C-O-C stretching (asym)
	750	s	C-H out of plane (bending of aromatic)

Table 3.3 ^{1}H NMR spectral data for the synthesized compounds

Compound	Chemical shifts[a]
Salen	3.8 (singlet,-CH_2-CH_2-,4H)
	6.8-7.3 (multiplet, aromatic,8H)
	8.3 (singlet,-CH=N-,2H)
	13.2 (singlet,-OH, 2H)
Saltn	1.9-2.1 (quintet,-CH_2-,2H)
	3.5-3.7 (triplet,N-CH_2-,4H)
	6.7-7.3 (multiplet,aromatic,8H)
	8.2 (singlet,-CH=N-,2H)
	13.4 (singlet,-OH,2H)
O-en	4.5 (singlet,-CH_2CH_2- , 4H)
	6.9-7.9 (multiplet, aromatic,8H)
	10.4 (singlet,-CHO,2H)
O-tn	2.3-2.5 (quintet,-CH_2-,2H)
	4.2-4.4 (triplet,O-CH_2-,4H)
	7.4-7.9 (multiplet,aromatic,8H)
	10.5 (singlet,CHO, 2H)

Table 3.3 (continued)

Compound	Chemical shifts[a]
O-en-N-tn	2.2 (quintet,-CH_2, 2H) 3.5-3.6 (triplet, N-CH_2-, 4H) 4.4 (singlet,O-CH_2-,4H) 6.9-8.0 (multiplet,aromatic,8H) 8.7 (singlet,CH=N,2H)
O-tn-N-tn	2.1-2.4 (multiplet,-CH_2-,4H) 3.5-3.7 (triplet,N-CH_2-,4H) 4.1-4.4 (multiplet,O-CH_2-4H) 6.9-8.8 (multiplet,aromatic,8H) 8.7 (singlet,-CH=N-,2H)

[a]All resonances in ppm downfield from TMS. $CDCl_3$ was used as solvent in each case.

Table 3.4 ^{13}C NMR spectral data for the synthesized compounds

Compound	Chemical shift	assignment
Salen	59.6	CH_2-N carbon
	116.9	aromatic carbons
	118.6	
	118.7	
	131.4	
	132.3	
	161.0	
	166.4	CH=N carbon
Saltn	31.6	-CH_2- carbon
	56.7	CH_2-N carbon
	116.8	aromatic carbons
	118.5	
	118.7	
	131.2	
	132.2	
	161.1	
	165.3	CH=N carbon

Table 3.4 (continued)

Compound	Chemical shift	assignment
O-en	67.2	CH_2-O- carbon
	112.9	C-3 |
	121.4	C-5 | aromatic carbons
	125.2	C-6 |
	128.4	C-4 |
	135.9	C-2 |
	160.8	C-1 |
	189.2	CHO carbon
O-tn	28.9	CH_2-carbon
	64.5	-CH_2-O- carbon
	112.3	C-3 |
	120.7	C-5 |
	124.7	C-6 | aromatic carbons
	128.4	C-4 |
	135.8	C-2 |
	160.8	C-1 |
	189.1	CHO carbon

Table 3.4 (continued)

Compound	Chemical shift	assignment
O-en-N-tn	28.6	$-CH_2$ - carbon
	57.9	$-CH_2$-N-carbon
	68.1	$-CH_2$-O carbon
	113.6	C-3
	121.8	C-5
	125.7	C-6 aromatic carbons
	127.1	C-4
	131.7	C-2
	158.6	C-1
	158.8	CH=N- carbon
O-tn-N-tn	28.7	$-CH_2-CH_2$-N carbon
	29.5	$-CH_2-CH_2$-O carbon
	57.1	$-CH_2$-N- carbon
	68.3	$-CH_2$-O- carbon
	112.7	C-3
	121.2	C-5
	125.4	C-6 aromatic carbons
	127.4	C-4
	131.7	C-2
	157.2	C-1
	158.7	CH=N- carbons

Table 3.5 Major features of the synthesized compound mass spectral fragmentation patterns.

Salen		Saltn	
m/e	fragment ions	m/e	fragment ions
268[a]	M.I.	282	M.I.
147	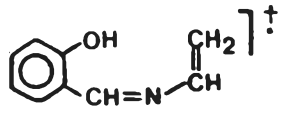	148[a]	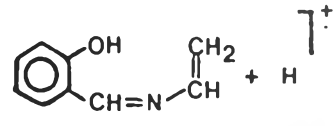
134	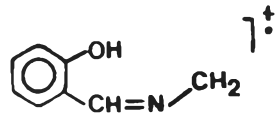	135	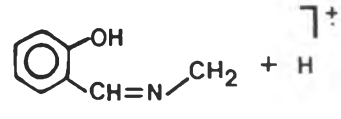
122	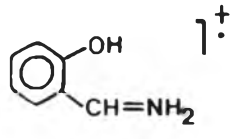	134	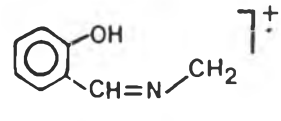
107		107	
79	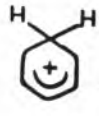	79	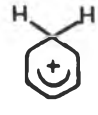
78	$C_6H_5^+ + \cdot H$	78	$C_6H_5^+ + \cdot H$
77	$C_6H_5^+$	77	$C_6H_5^+$
51	$C_4H_3^+$	51	$C_4H_3^+$

[a] the base peak

Table 3.5 (continued)

O-en		O-tn	
m/e	fragment ions	m/e	fragment ions
270	M.I.	284	M.I.
149	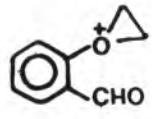	162	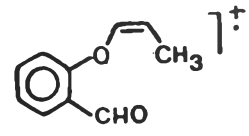
135	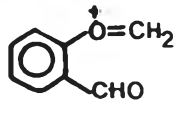	133	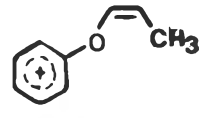
121[a]	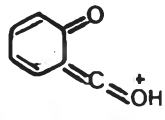	121[a]	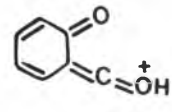
120	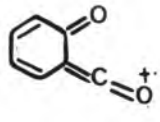	77	$C_6H_5^+$
93	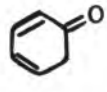	51	$C_4H_3^+$
77	$C_6H_5^+$		
65			
51	$C_4H_3^+$		

[a] the base peak

Table 3.5 (continued)

O-en-N-tn		O-tn-N-tn	
m/e	fragment ions	m/e	fragment ions
308	M.I.	322[a]	M.I.
280	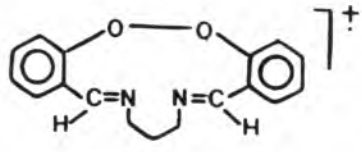	294	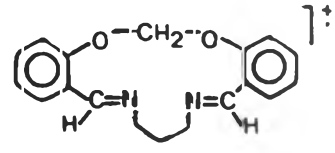
162[a]	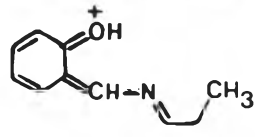	293	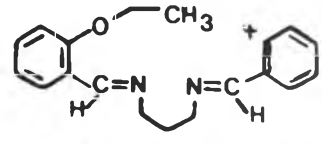
146	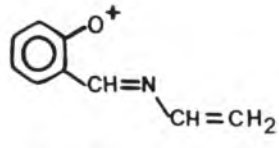	279	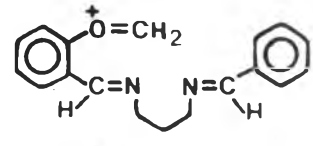
134	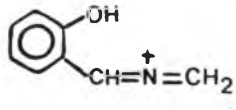	162	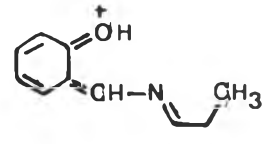
107		148	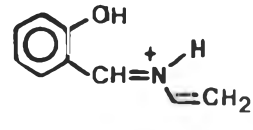
77	$C_6H_5^+$	134	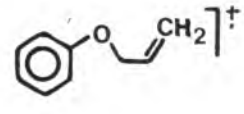
51	$C_4H_3^+$	107	
		91	
		77	$C_6H_5^+$
		51	$C_4H_3^+$

[a] the base peak

Table 3.6 Elemental analysis data for the synthesized compounds.

Compound	%C		%H		%N	
	Calcd	Found	Calcd	Found	Calcd	Found
Salen	71.64	71.61	5.97	6.05	10.45	10.41
Saltn	72.34	72.19	6.38	6.35	9.93	9.73
O-en	71.11	71.04	5.19	5.23	-	-
O-tn	71.83	71.73	5.63	5.75	-	-
O-en-N-tn	74.03	74.19	6.49	6.62	9.09	9.08
O-tn-N-tn	74.53	74.53	6.88	6.88	8.70	8.85

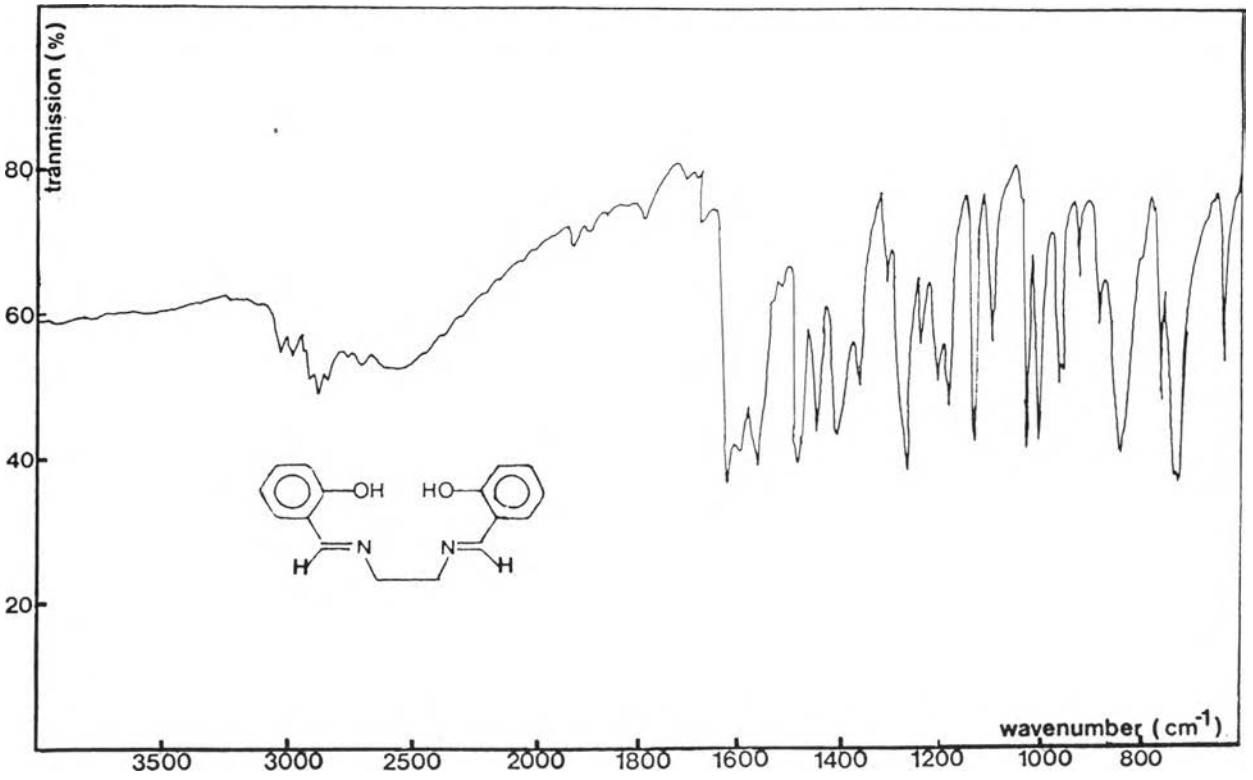

Fig 3.1 :IR spectrum of Bis(salicylaldehyde)*N,N'*-ethylenediimine in KBr;Salen

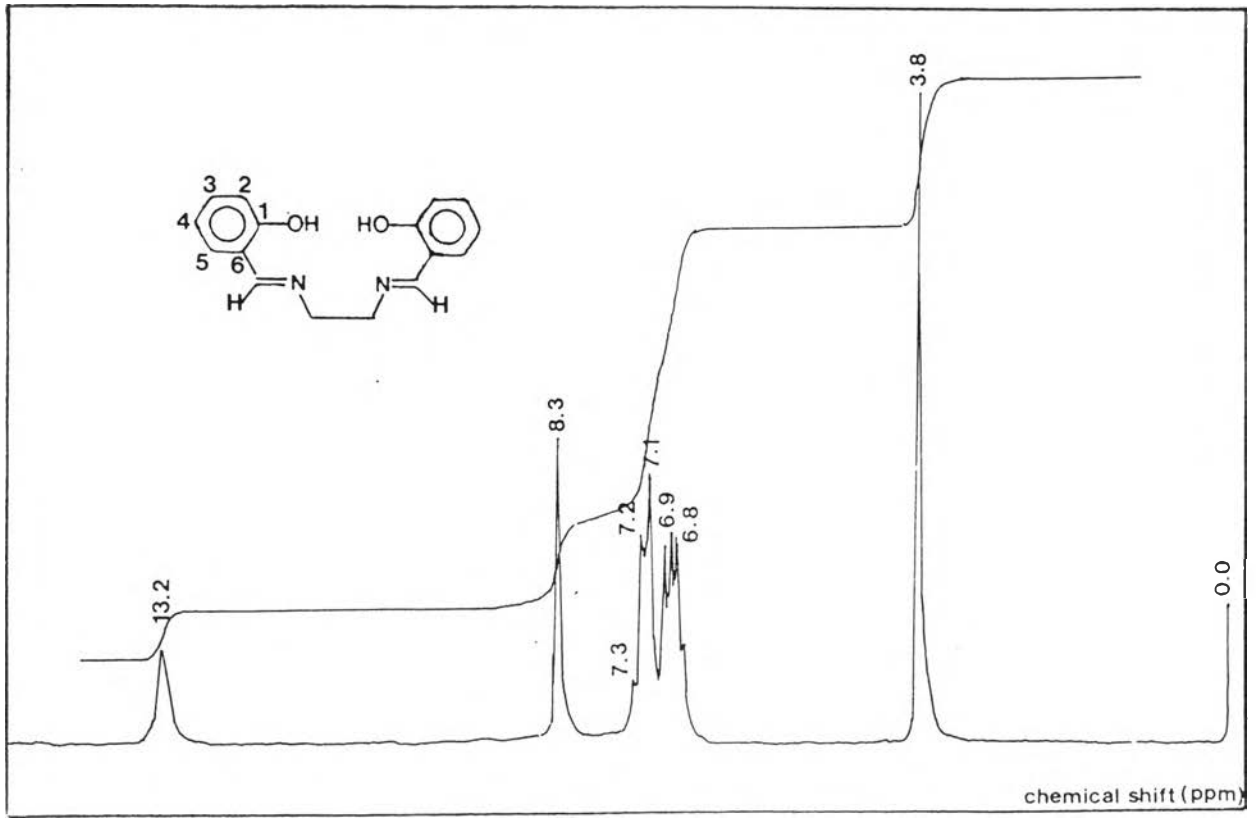

Fig 3.2 : ^{1}H NMR spectrum of Bis(salicylaldehyde)*N*,*N*′-ethylenediimine in $CDCl_3$;Salen

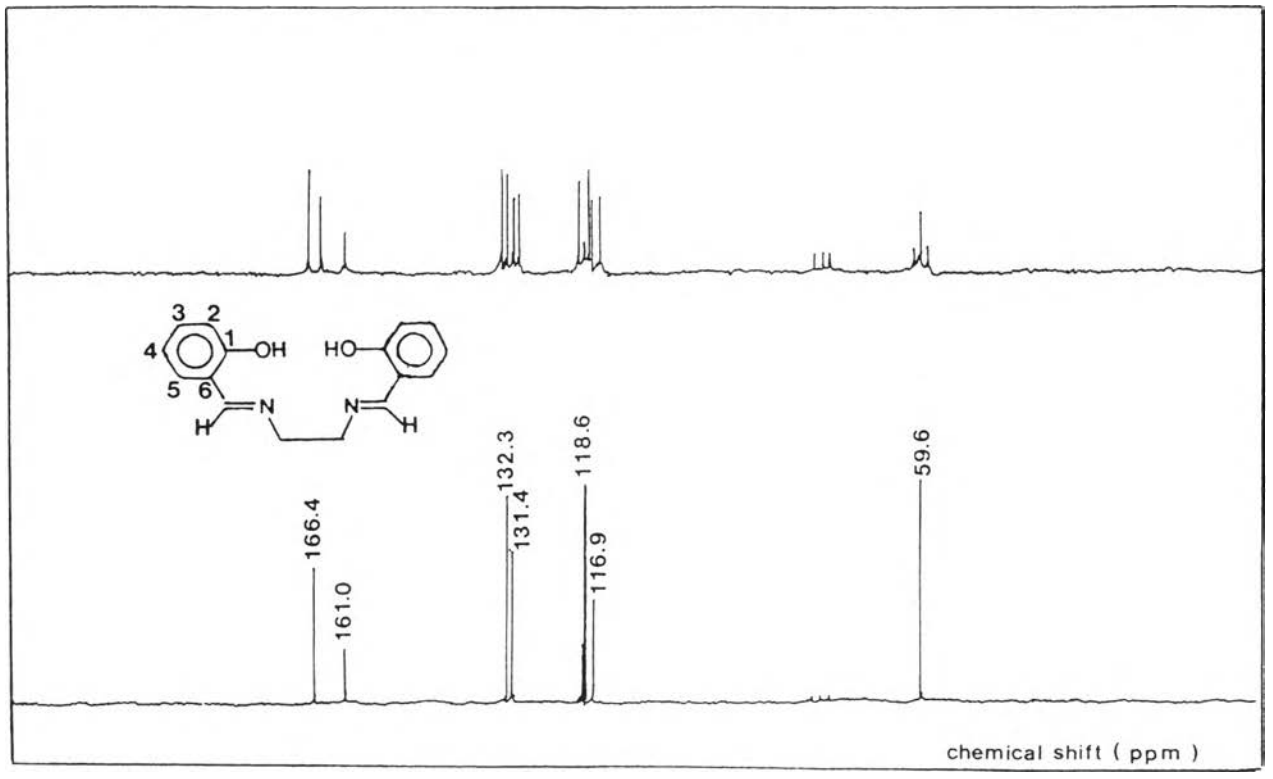

Fig 3.3 :^{13}C NMR spectrum of Bis(salicylaldehyde)*N,N'*-ethylenediimine in $CDCl_3$;Salen

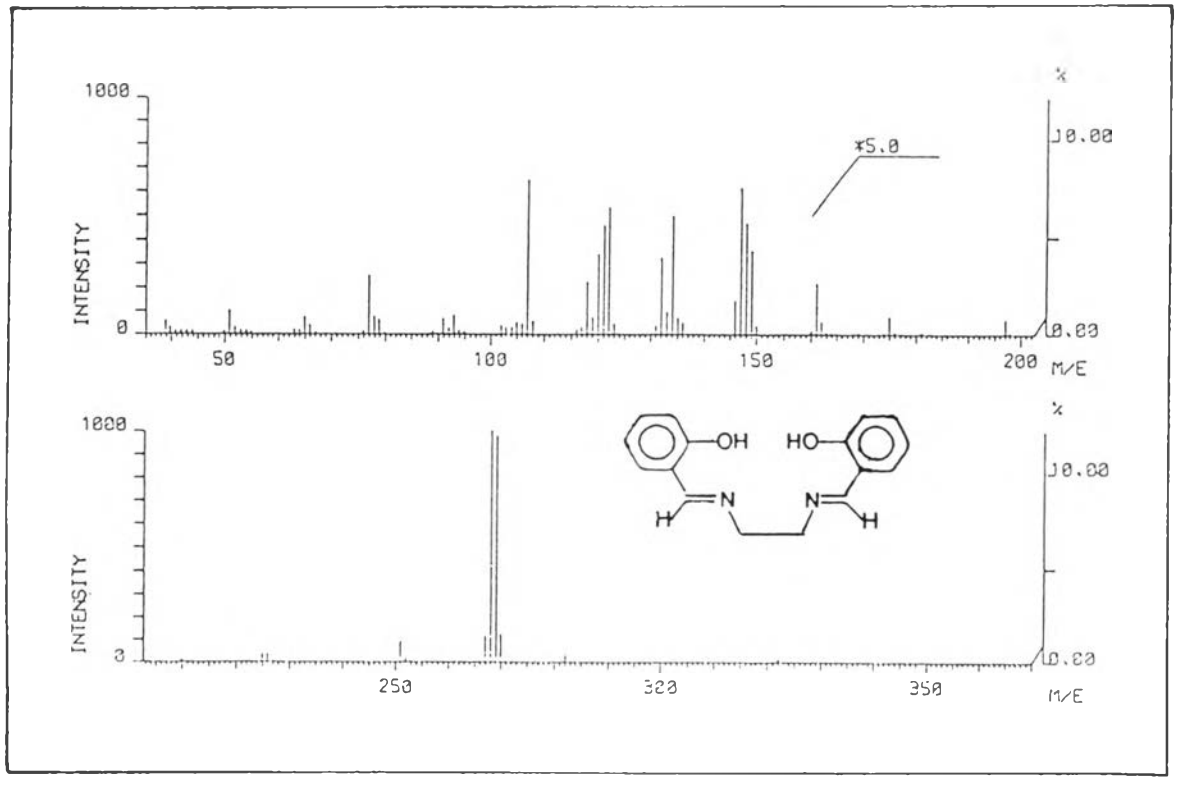

Fig 3.4 :Mass spectrum of Bis(salicylaldehyde)*N,N'*-ethylenediimine ;Salen

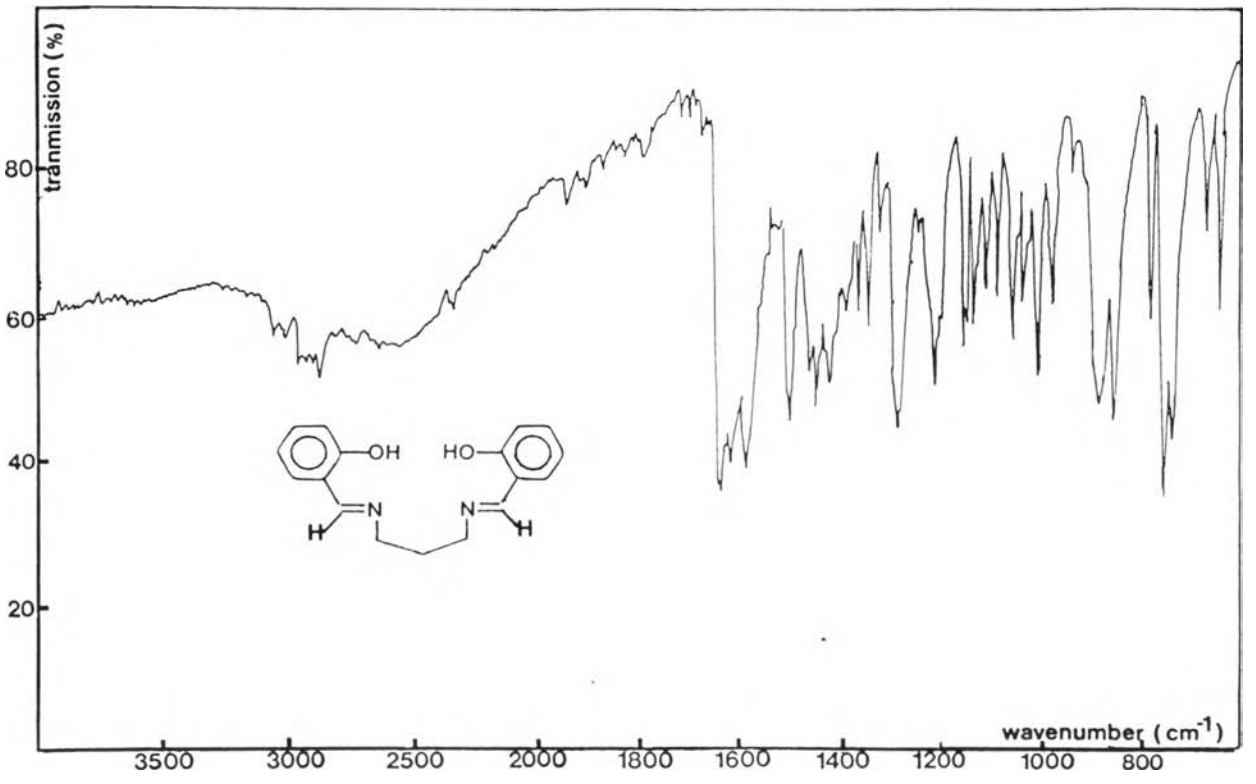

Fig 3.5 :IR spectrum of Bis(salicylaldehyde)*N,N'*-trimethylenediimine in KBr;Saltn

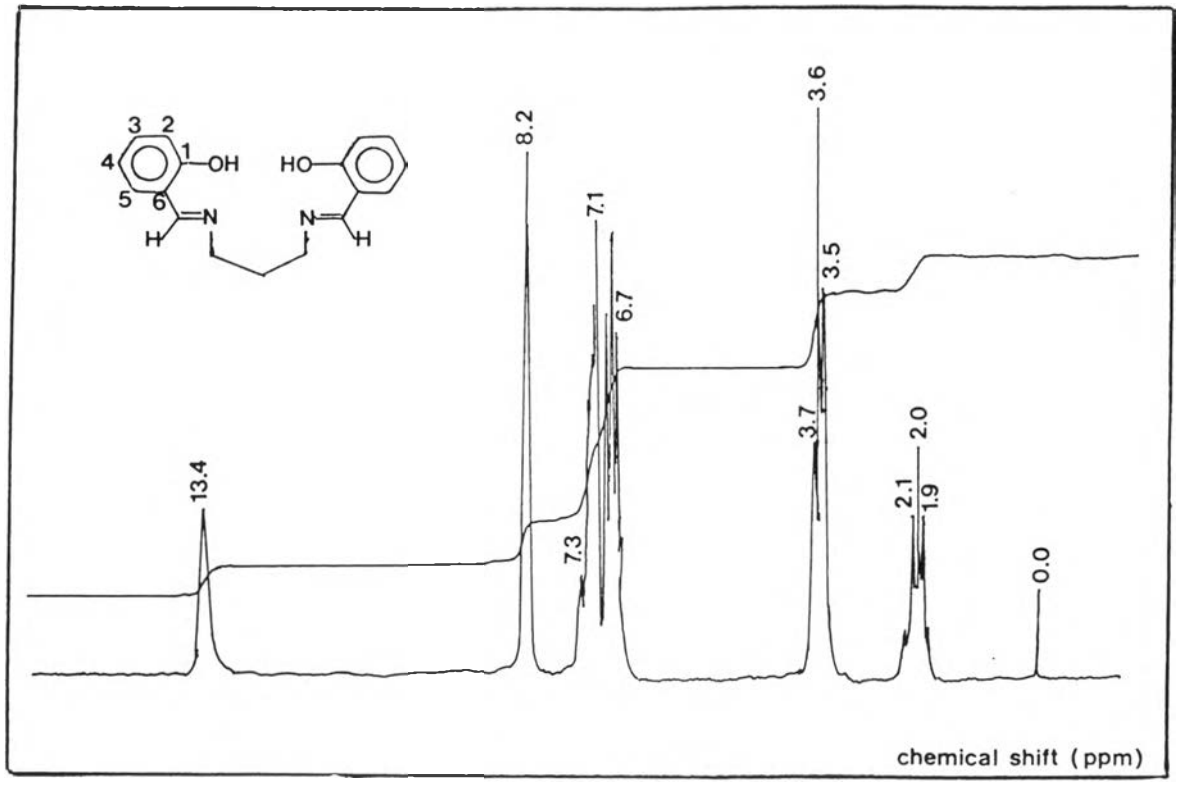

Fig 3.6 : ^{1}H NMR spectrum of Bis(salicylaldehyde)*N,N'*-trimethylenediimine in $CDCl_3$; Saltn

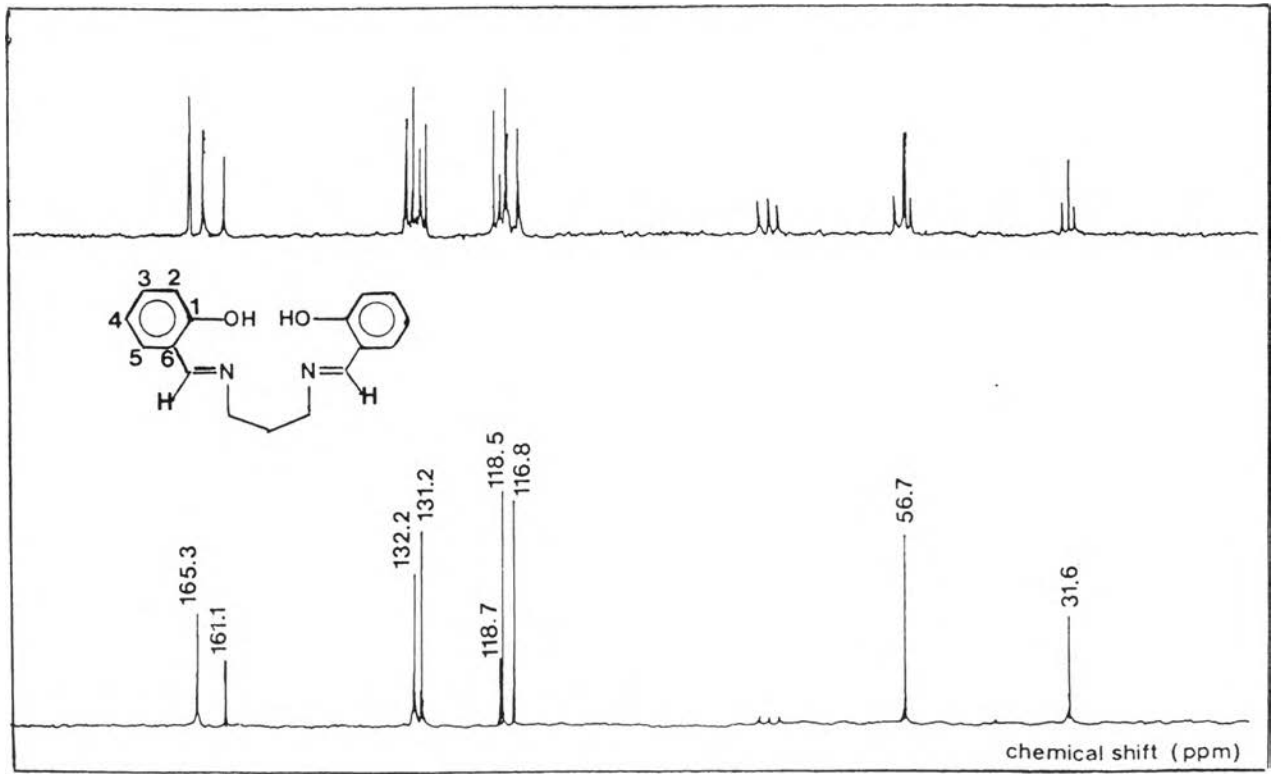

Fig 3.7 : ^{13}C NMR spectrum of Bis(salicylaldehyde)*N,N'*-trimethylenediimine in $CDCl_3$; Saltn

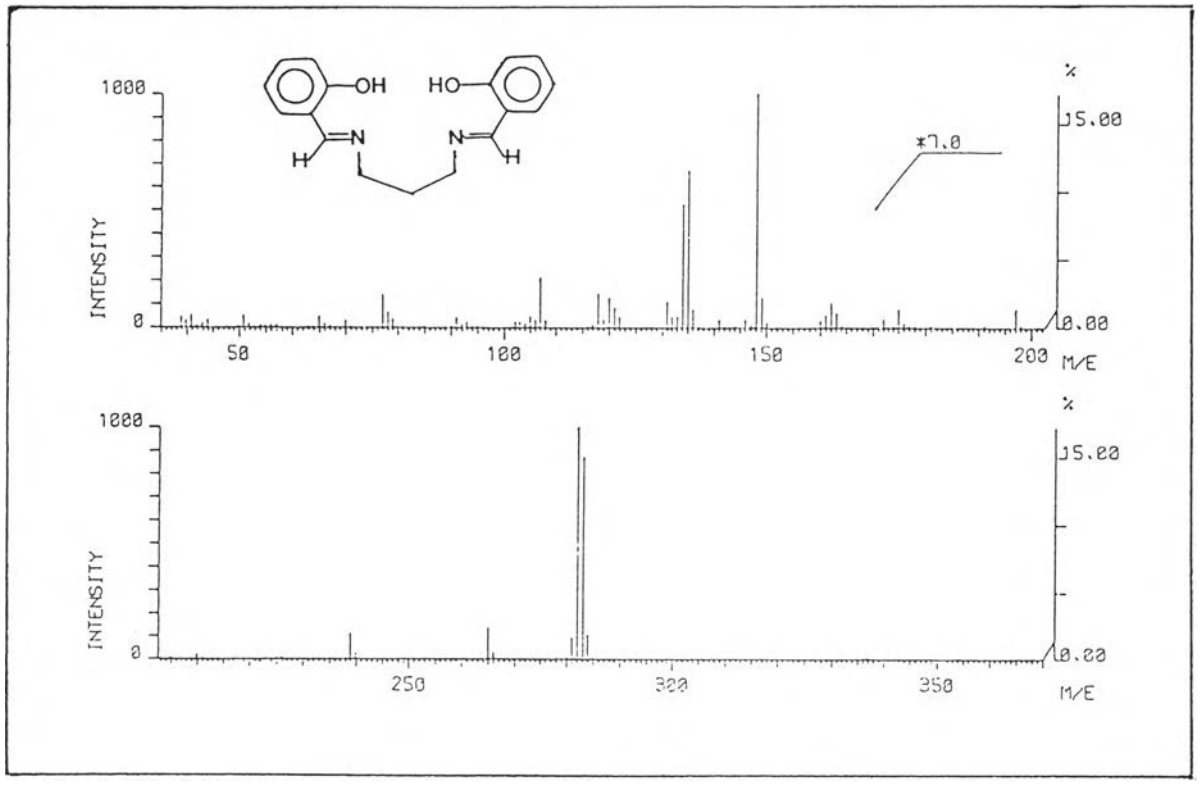

Fig 3.8 :Mass spectrum of Bis(salicylaldehyde)*N,N'*- trimethylene diimine ; Saltn

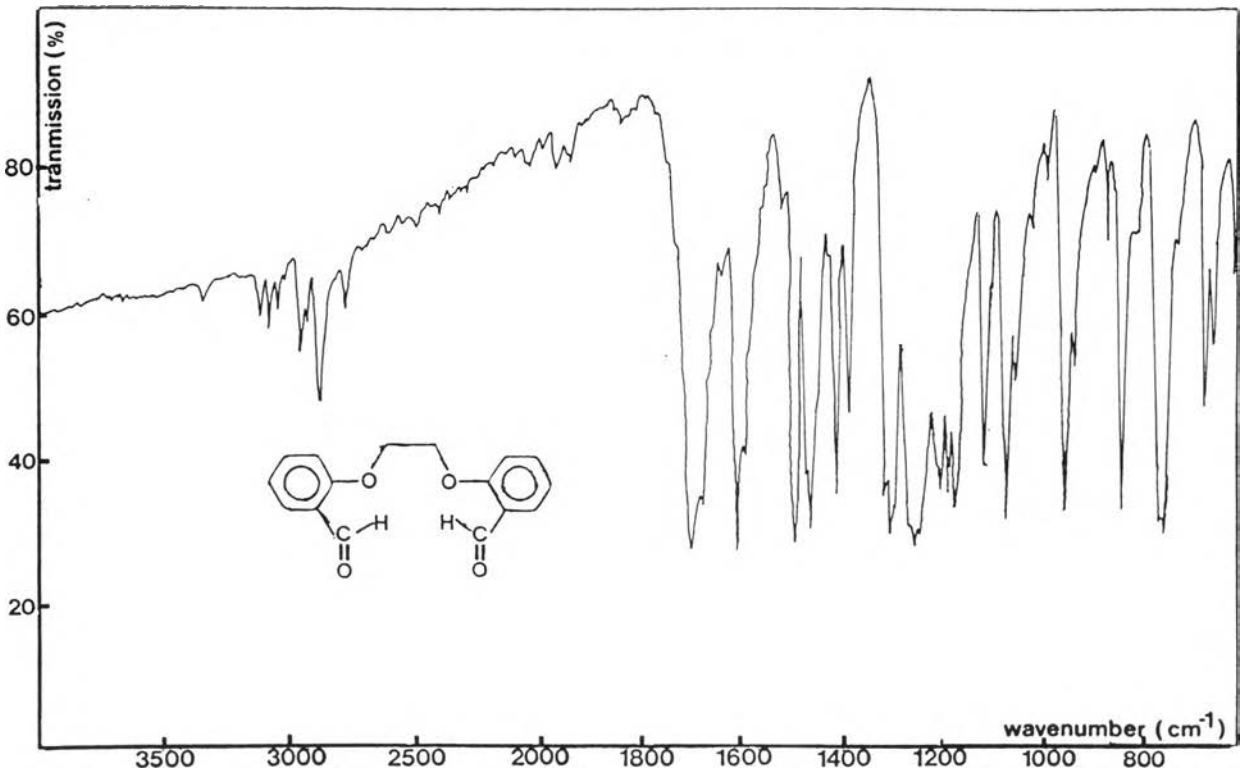

Fig 3.9 :IR spectrum of 1,4-Bis (2/-formylphenyl)-1,4-dioxabutane in KBr ; O-en

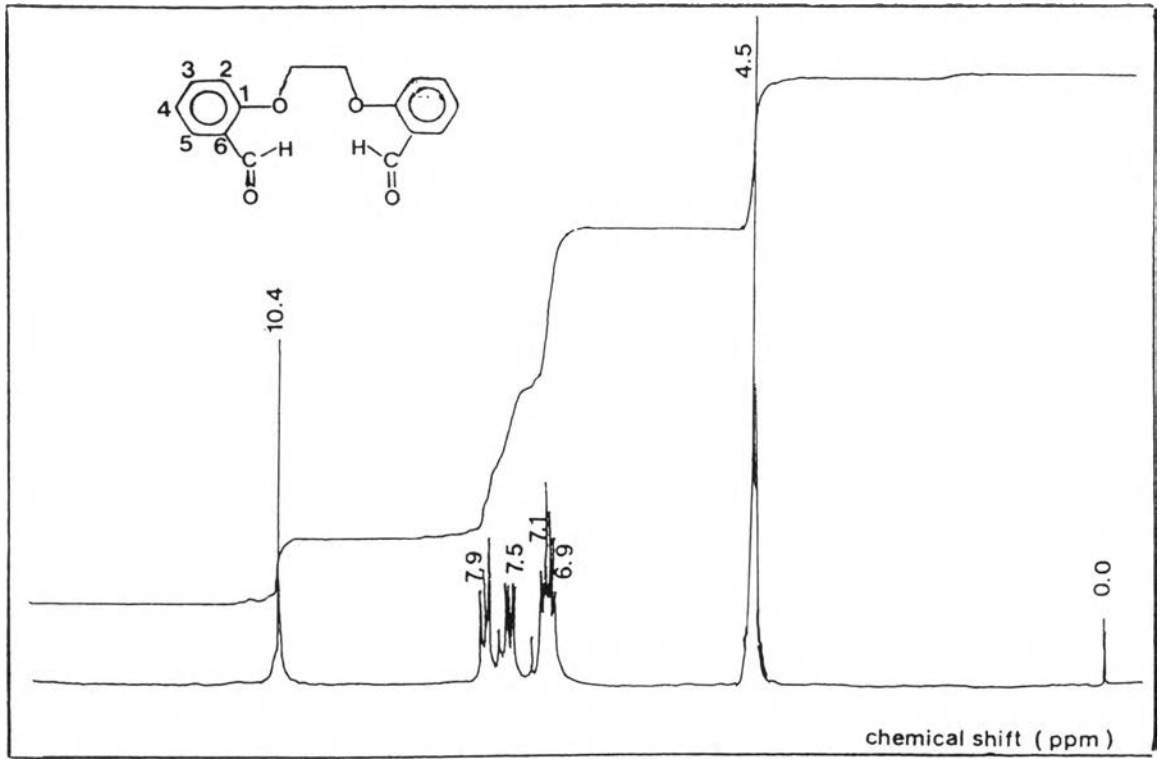

Fig 3.10 : ^{1}H-NMR spectrum of 1,4-Bis (2′-formylphenyl)-1,4-dioxabutane in $CDCl_3$; O-en

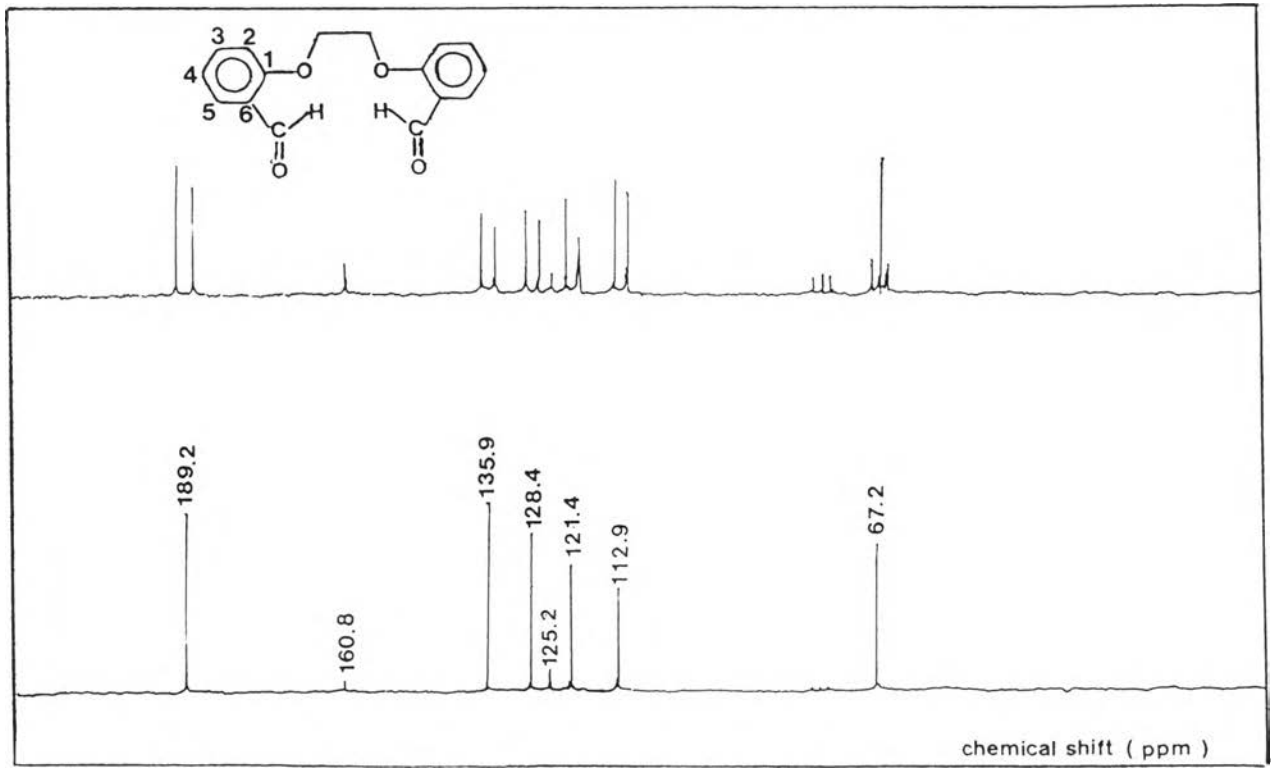

Fig 3.11 : ^{13}C-NMR spectrum of 1,4-Bis (2/-formylphenyl)-1,4-dioxabutane in $CDCl_3$; O-en

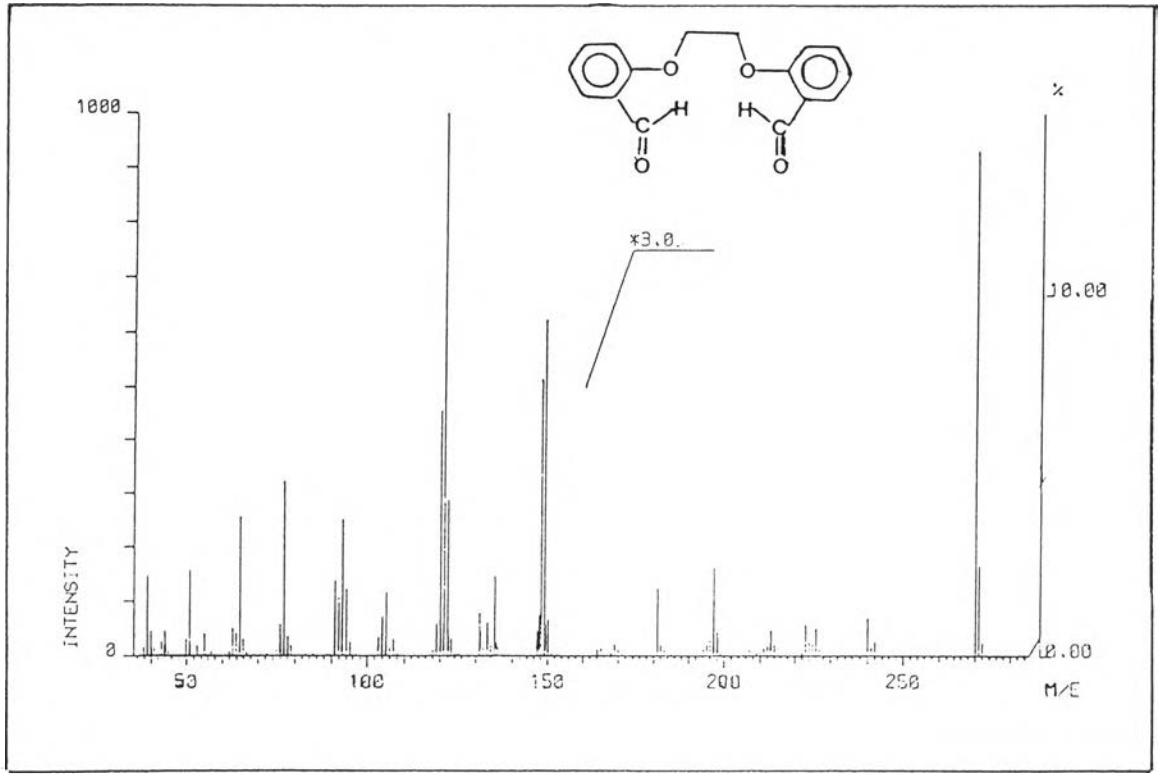

Fig 3.12 :Mass spectrum of 1,4-Bis (2/-formylphenyl)-1,4-dioxabutane ; O-en

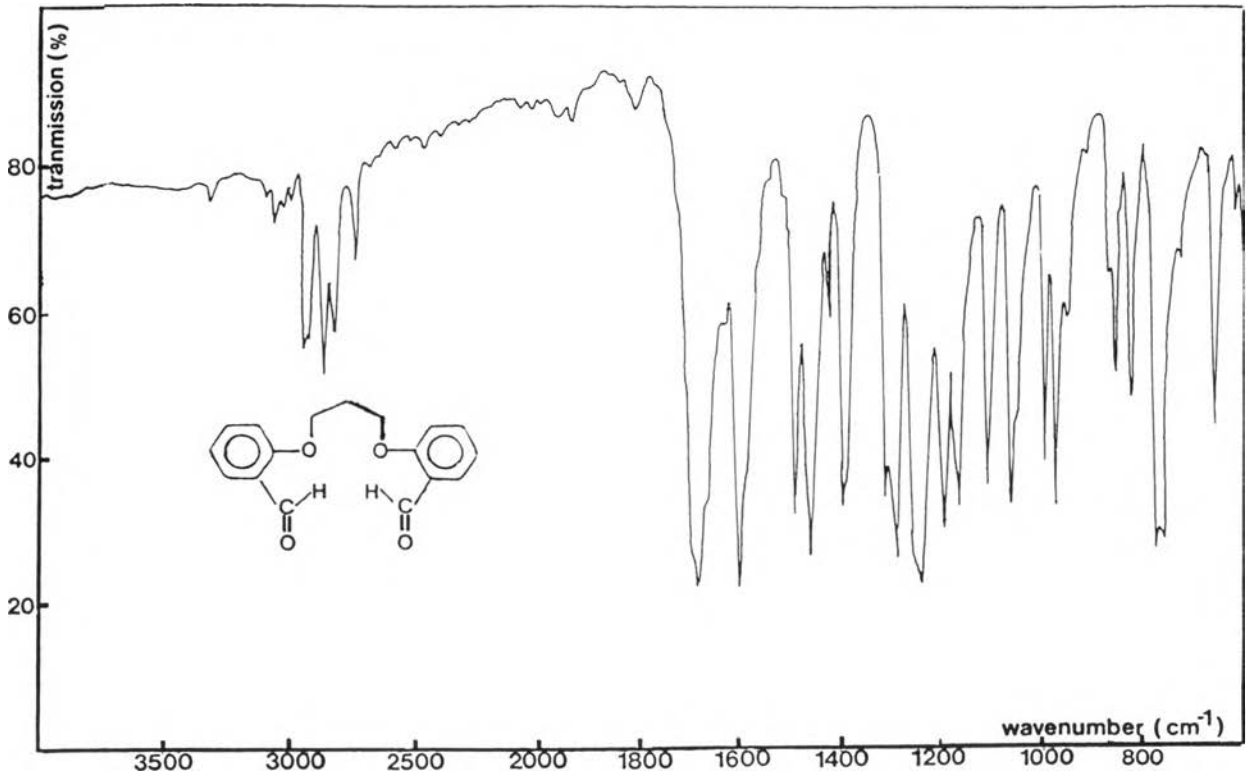

Fig 3.13 :IR spectrum of 1,5-Bis (2/-formylphenyl)-1,5-dioxapentane in KBr; O-tn

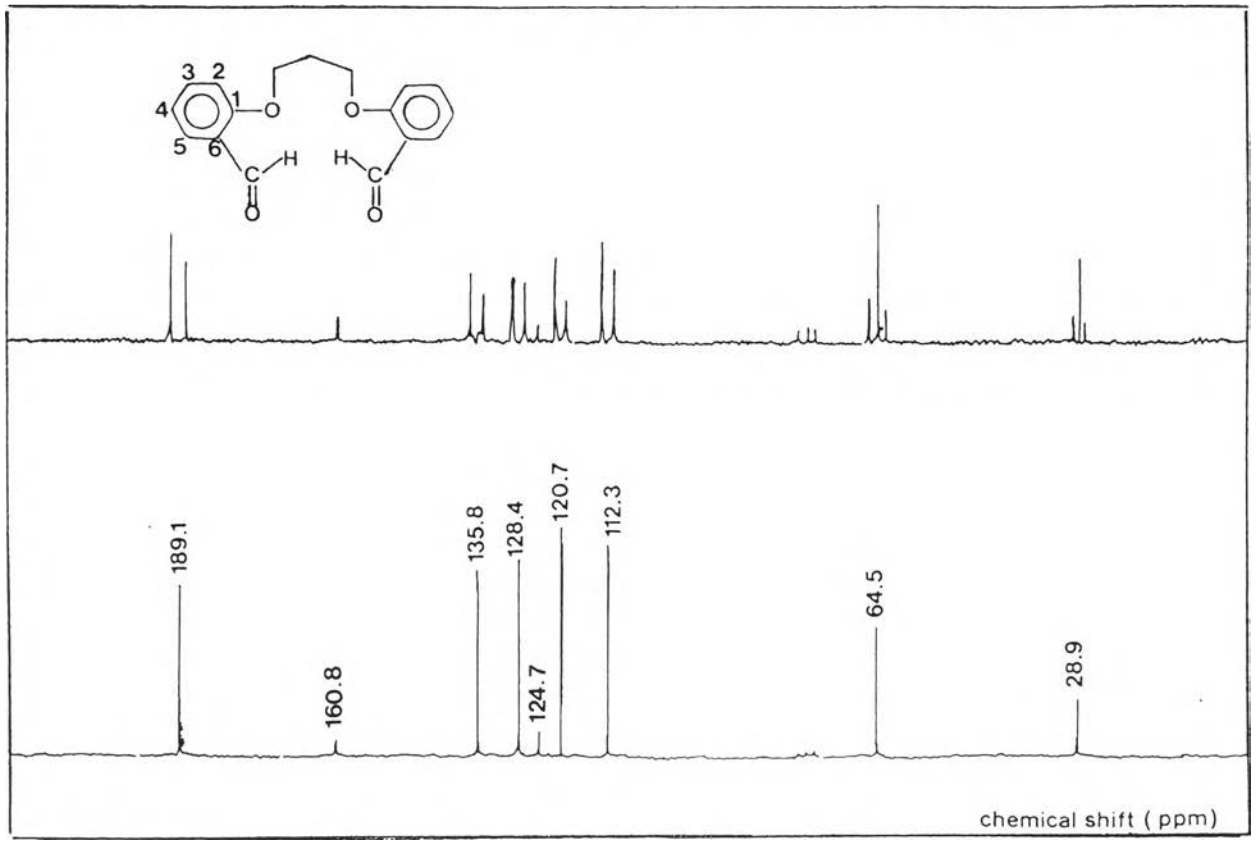

Fig 3.15 : ^{13}C NMR spectrum of 1,5-Bis (2-formylphenyl)-1,5-dioxapentane in $CDCl_3$; O-tn

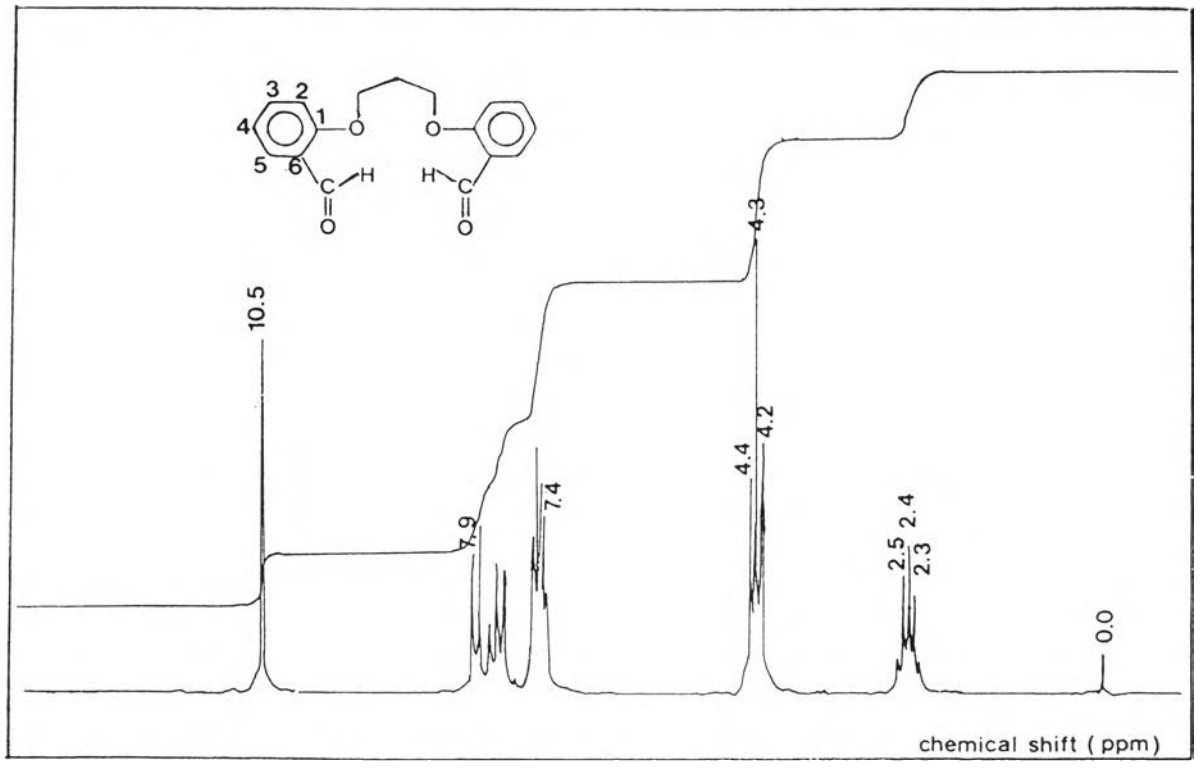

Fig 3.14 : ^1H NMR spectrum of 1,5-Bis (2-formylphenyl)-1,5-dioxapentane in $CDCl_3$; O-tn

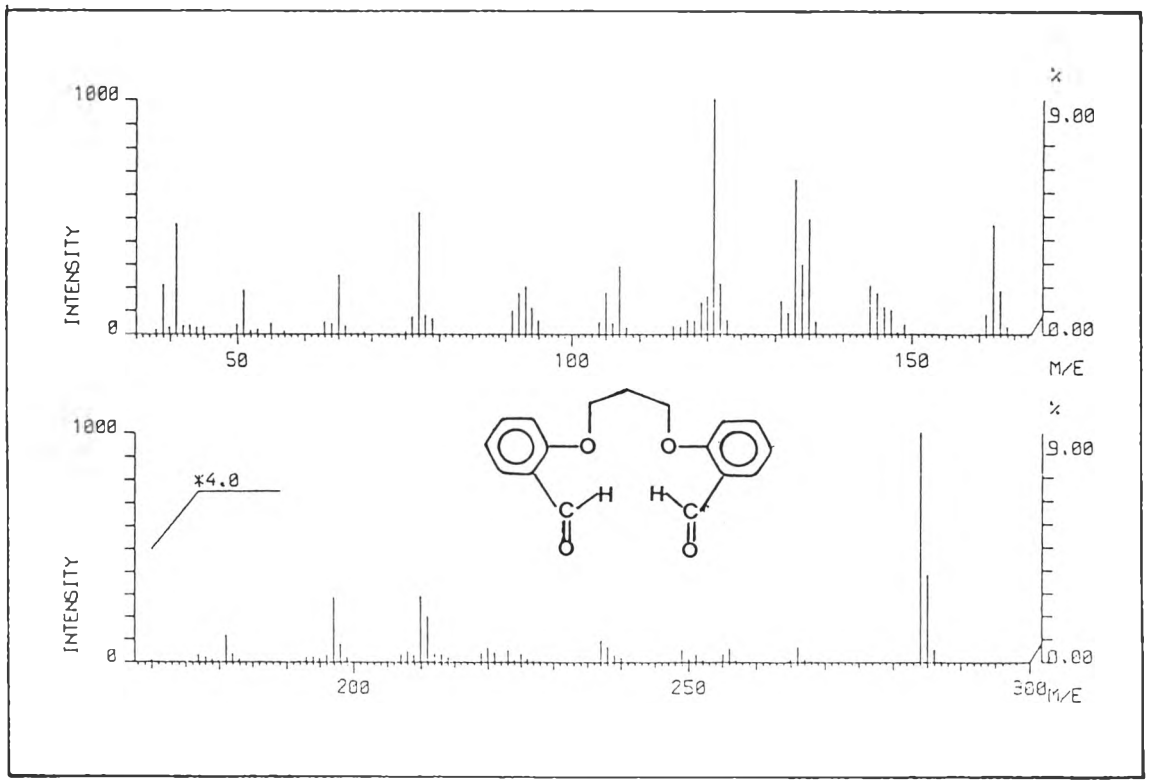

Fig 3.16 :Mass spectrum of 1,5-Bis (2-formylphenyl)-1,5-dioxapentane ;O-tn

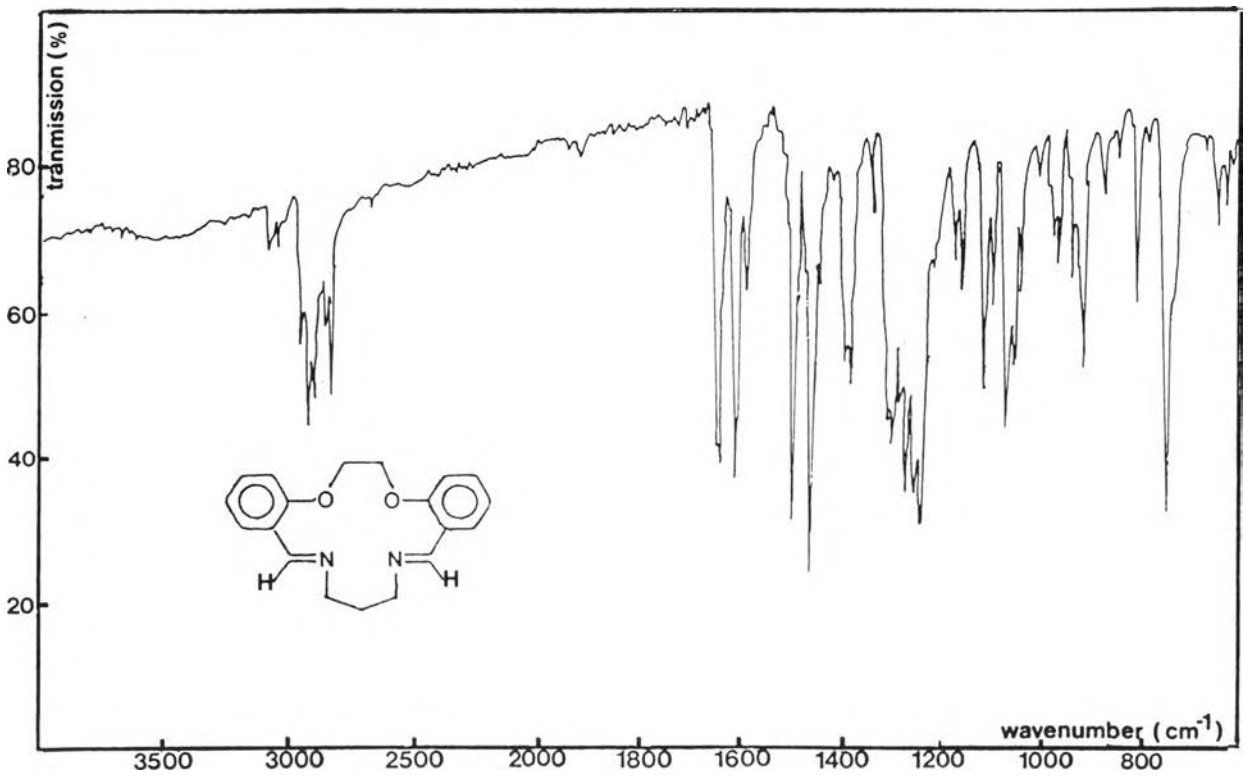

Fig 3.17 : IR spectrum of 3,4,9,10-Dibenzo-1,12-diaza-5,8-dioxacyclopentadecane-1,11-diene in KBr;O-en-N-tn

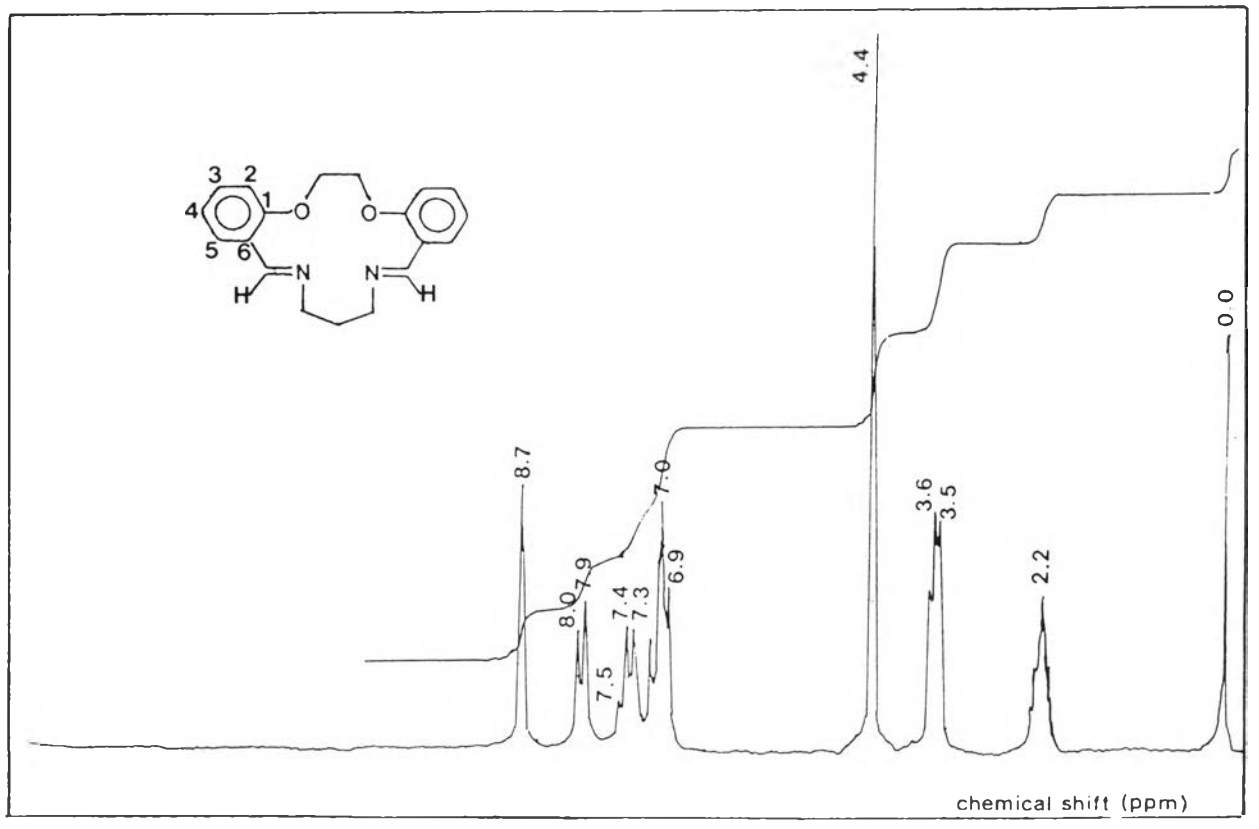

Fig 3.18 : ^{1}H NMR spectrum of 3,4,9,10-Dibenzo-1,12-diaza-5-8-dioxacyclopentadecane-1,11-diene in $CDCl_3$;O-en-N-tn

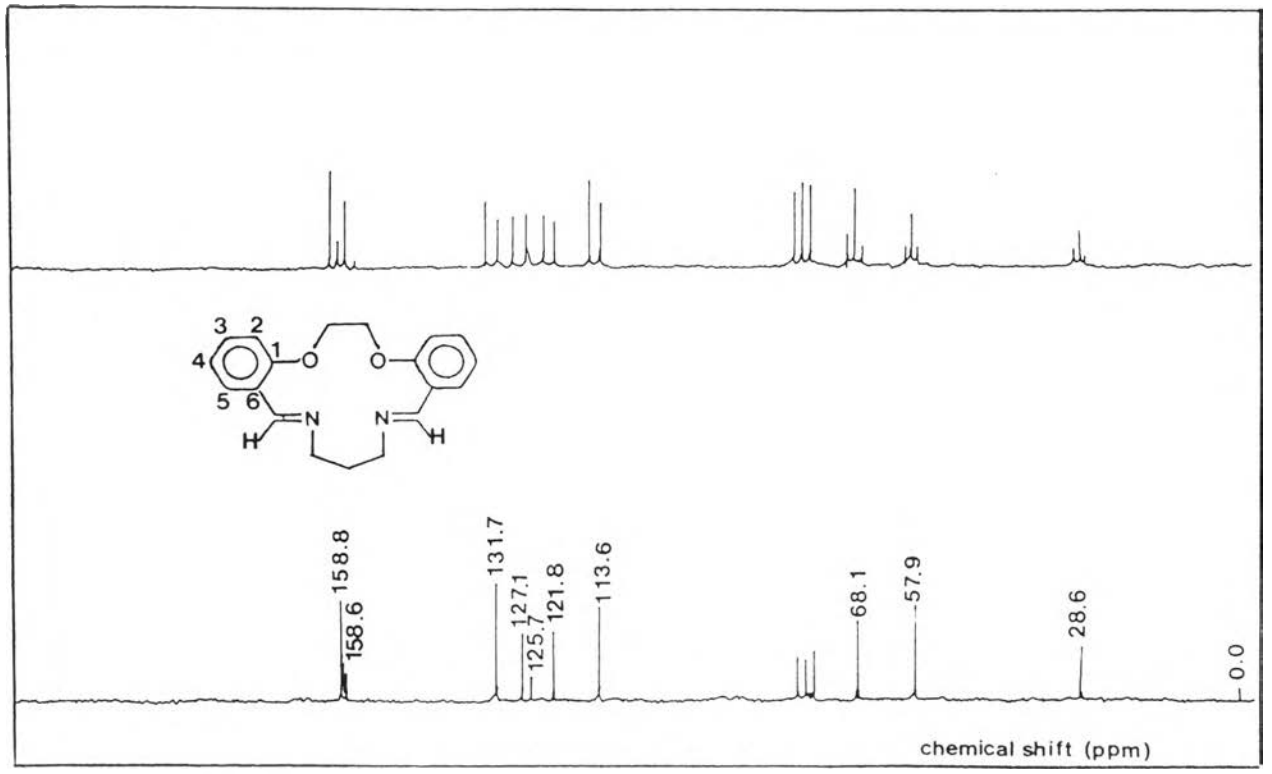

Fig 3.19 : ^{13}C NMR spectrum of 3,4,9,10-Dibenzo-1,12-diaza-5-8-dioxacyclopentadecane-1,11-diene in $CDCl_3$;O-en-N-tn

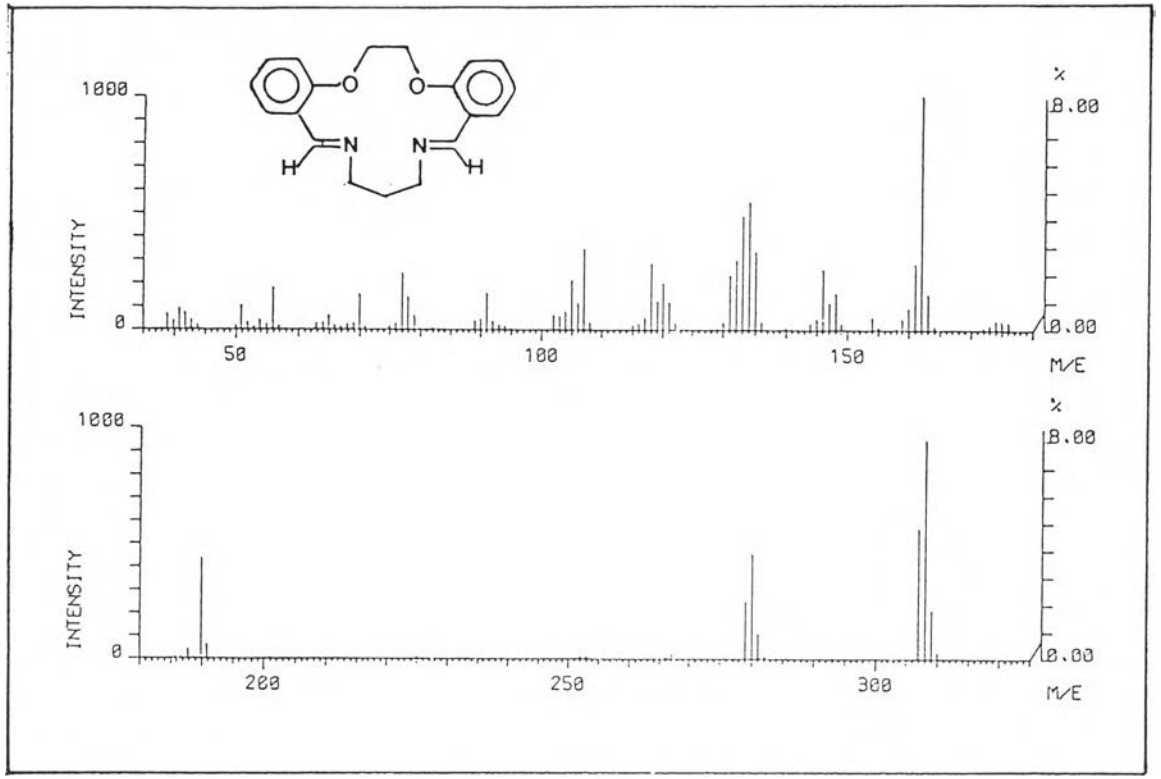

Fig 3.20 : Mass spectrum of 3,4,9,10-Dibenzo-1,12-diaza-5,8-dioxacyclopentadecane-1,11-diene ; O-en-N-tn

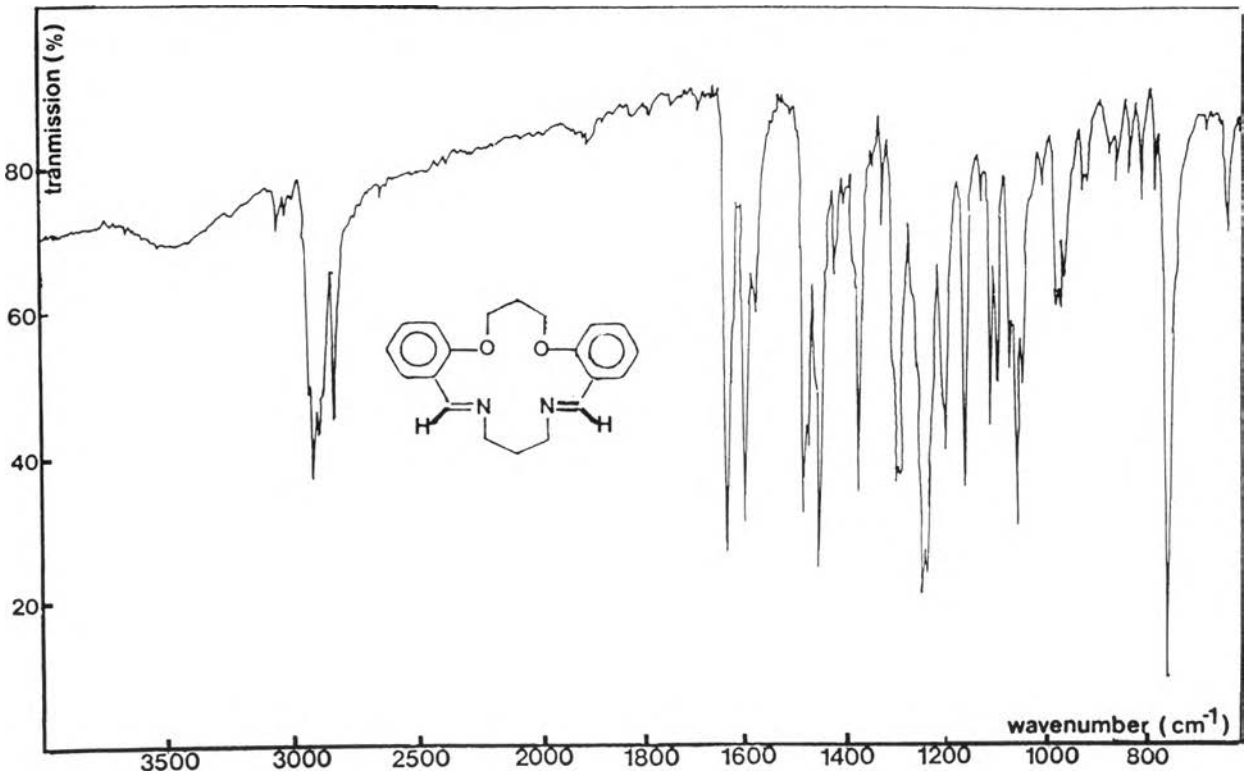

Fig 3.21 : IR spectrum of 3,4,10,11-Dibenzo-1,13-diaza-5,9-dioxacyclohexadecane-1,12-diene in KBr;O-tn-N-tn

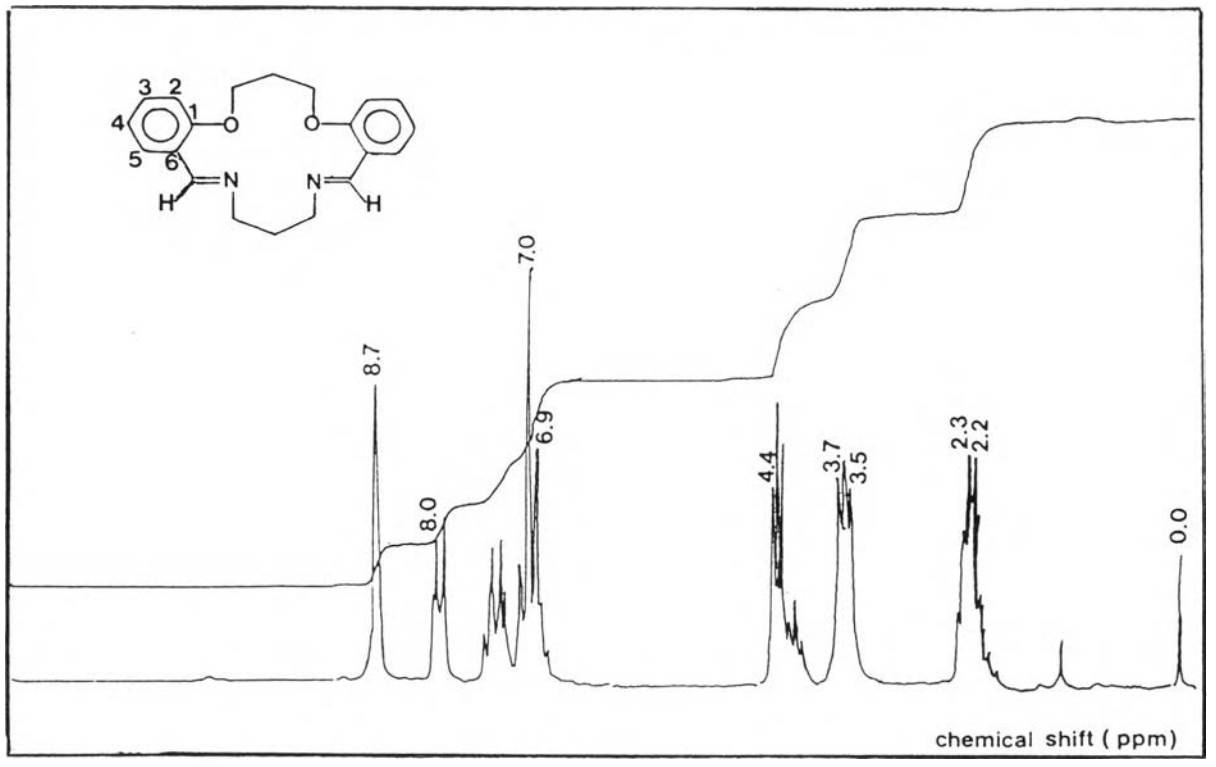

Fig 3.22 : ^{1}H NMR spectrum of 3,4,10,11-Dibenzo-1,13-diaza-5,9-dioxacyclohexadecane-1,12-diene in $CDCl_3$; O-tn-N-tn

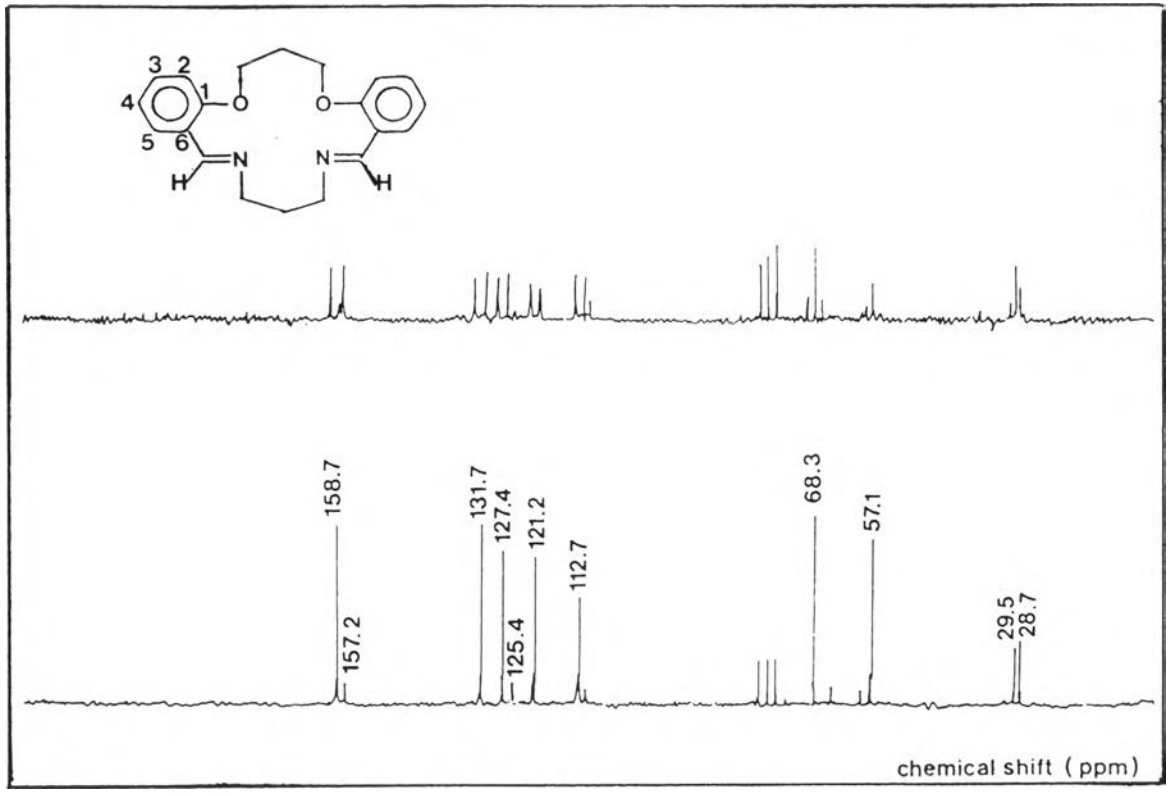

Fig 3.23 : ^{13}C NMR spectrum of 3,4,10,11-Dibenzo-1,13-diaza-5,9-dioxacyclohexadecane-1,12-diene in $CDCl_3$; O-tn-N-tn

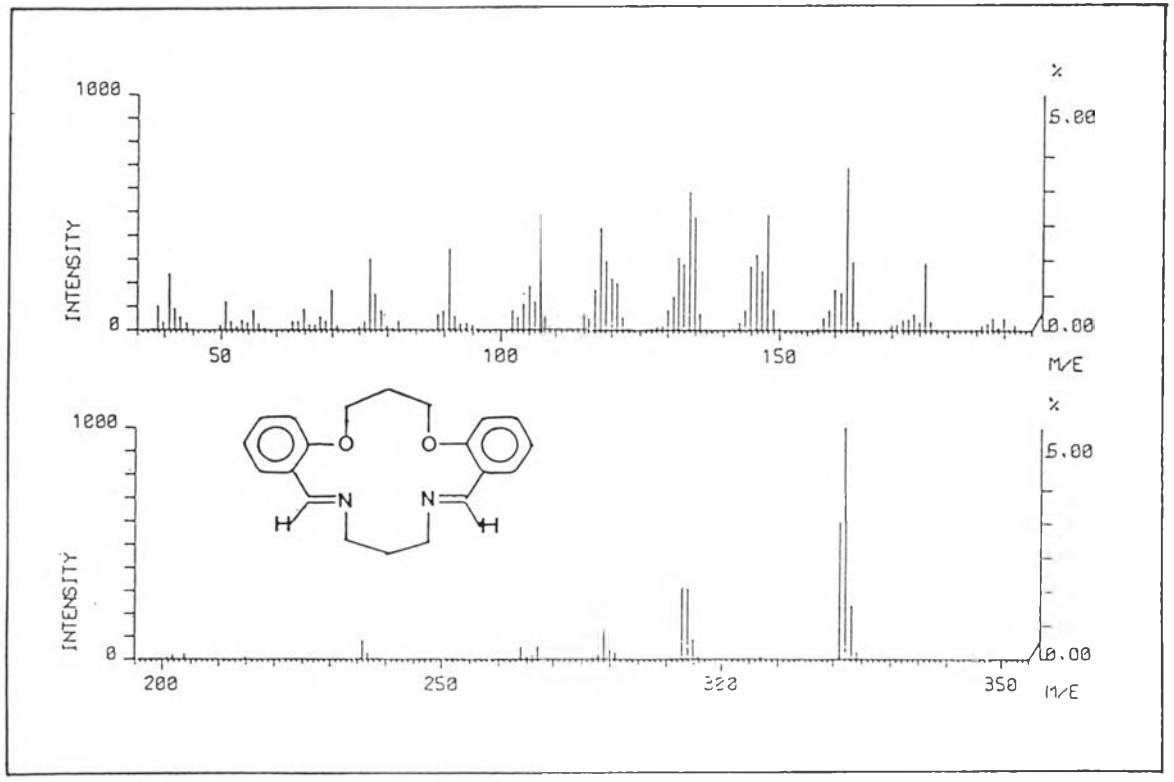

Fig 3.24 : Mass spectrum of 3,4,10,11-Dibenzo-1,13-diaza-5,9-dioxacyclohexadecane-1,12-diene ;O-tn-N-tn

3.3 Cation Binding Property and Complex Formation Study

3.3.1 Solvent Extraction

It was likely that crown ethers form strong complex with hard cations such as alkali or alkaline earth metal ions. However,aza-crown ethers were expected to possess affinity for soft cations such as transition or heavy metals. Also,the cation-complexing selectivity depended on the cavity size,type of metal ions,kinds of donor atoms and some other factors,discussed in Chapter I. In this study,these following cations were selected for investigations ; Cr^{3+}, Mn^{2+}, Cd^{2+},Cu^{2+},Co^{2+},Ni^{2+} and Pb^{2+}.

The cation binding properties of the synthesized ligands were investigated by shaking these metal ions with the synthetic ligand,as described in section 2.2.1. Each ligand was studied with the selected metal ions and the decrease in the metal ion concentration in the aqueous phase was measured by atomic absoption spectrophotometric method. The results of solvent extraction in chloroform / aqueous phase system at various pH's were shown in Table 3.7. All extraction conditions were kept constant throughout the experiment so that the data obtained for each metal ion could be compared.

For open ring ligands,it appeared that the percent

extraction,for each metal,increases with the increase of the pH value. It can also be generalized that the trend of cation binding ability of the open ring ligands was very low at pH < 4.5. This is also the case for Cu^{2+} ion whose percent extraction at pH 4.5 is much higher than those of lower pH's. Some metals such as Mn^{2+} and Cr^{3+} ions were not examined at pH > 7.2 due to metal hydroxide precipitation,while Co^{2+} and Ni^{2+} ions showed their best extracting performance at pH > 7.2. It was believed that the greater K_{sp} values for the latter metal hydroxides than those for the former ones were responsible for this observation. The pH of the aqueous solution seemed to have more pronounced effect for the extraction with the macrocyclic ligands. No general trend could be made for these macrocyclic ligands as for the open ring ligands in the foregoing discussion. However, both compounds seemed to show better extracting performance at higher pH values (7.2-8.1). But in all cases,the percent extracting values were considered very small. This could be due to the ionic character of the obtained complex species (see Scheme IV),in contrast to the neutral character of the complex species when the ligand was the open ring compound,which would not likely go into the organic phase readily. An attempt to achieve a better extracting performance was also made by adding a large anion into the aqueous phase e.g. picrate ion,BF_4^-, but no improvment was observed.

Table 3.7 Percent extraction data of various metal ions by using Schiff-base ligand[a]

Metal	Ionic size Å	pH of aqueous phase[c]	Percent Extraction[b]			
			Salen	Saltn	O-en-N-tn	O-tn-N-tn
Cr^{3+}	1.38	2.2	1.14	0.43	1.67	0.66
		3.4	5.84	6.10	6.09	6.43
		4.5	5.30	6.28	7.92	8.92
		5.9	7.41	7.32	4.67	5.84
		7.2	13.04	11.97	10.55	11.19
Mn^{2+}	1.60	2.2	2.34	2.15	0.48	1.28
		3.4	2.15	2.14	0.98	1.19
		4.5	2.25	3.10	2.72	3.25
		5.9	2.34	2.37	1.96	2.25
		7.2	6.19	7.92	11.03	13.79
Cd^{2+}	1.94	2.2	0.00	0.81	0.43	0.38
		3.4	0.00	0.96	0.45	0.85
		4.5	1.83	2.88	0.54	1.38
		5.9	2.44	3.75	3.19	1.68
		7.2	2.44	2.88	3.38	3.38
		8.1	3.29	0.99	1.78	4.71
Cu^{2+}	1.78	2.2	55.69	39.76	0.05	0.00
		3.4	61.83	54.63	1.28	4.39
		4.5	99.05	77.83	11.81	2.06

Table 3.7 (continued)

Metal	Ionic size Å	pH of aqueous phase[c]	Percent Extraction[b]			
			Salen	Saltn	O-en-N-tn	O-tn-N-tn
		5.9	99.26	98.47	3.57	4.24
		7.2	99.58	63.37	15.25	17.70
		8.1	70.76	60.94	2.53	1.28
Co^{2+}	1.48	2.2	2.91	2.90	3.38	1.57
		3.4	6.34	2.54	6.54	5.57
		4.5	3.19	2.91	3.57	3.27
		5.9	8.76	5.57	8.24	11.35
		7.2	7.58	7.92	6.28	7.92
		8.1	31.22	24.24	19.81	21.26
Ni^{2+}	1.44	2.2	3.57	5.57	7.75	8.26
		3.4	9.42	9.67	8.26	8.24
		4.5	0.49	0.33	0.99	0.67
		5.9	9.42	10.55	9.26	8.00
		7.2	2.91	3.47	5.12	6.63
		8.1	23.55	20.00	15.97	13.79
Pb^{2+}	2.40	2.2	0.45	0.55	0.99	0.30
		3.4	0.55	0.25	0.49	0.59
		4.5	3.83	3.85	5.27	4.21
		5.9	4.21	3.47	5.35	4.40
		7.2	15.25	13.34	15.97	17.69
		8.1	1.77	1.30	4.76	4.94

[a] All data for liquid-liquid extraction were duplicate analysis

[b] calculation , see Appendix A

[c] see Table 2.1, chapter II

3.3.2 Stoichiometric and the Apparent Stability constant Study of Complex in Absolute Methanol

Cu^{2+} ion was chosen as a model for studies of stoichiometry and stability constant of complex with all ligands since it proved better results than the other ions. Absolute methanol was used as solvent since both Cu^{2+} ion and ligand could be dissolved to be a homogeneous solution. Job's method was employed in stoichiometric study and the selected wavelength for each case was 562,356,352 and 364 nm for Cu-Salen,Cu-Saltn,Cu-[O-en-N-tn] and Cu-[O-tn-N-tn], as shown in Figure 3.25,3.26,3.27 and 3.28 respectively. It was clearly seen , Figure 3.29 and 3.30, that Salen and Saltn bound to Cu^{2+} ion as 1:1 complex, O-en-N-tn and O-tn-N-tn form with Cu^{2+} ion as 2:1 complex. In addition, Figure 3.31 and 3.32,illustrated that O-tn-N-tn could be hydrolyzed more easily than O-en-N-tn . The apparent stability constants for all complexes were approximately calculated from the corresponding Job's plots as shown in Table 3.8

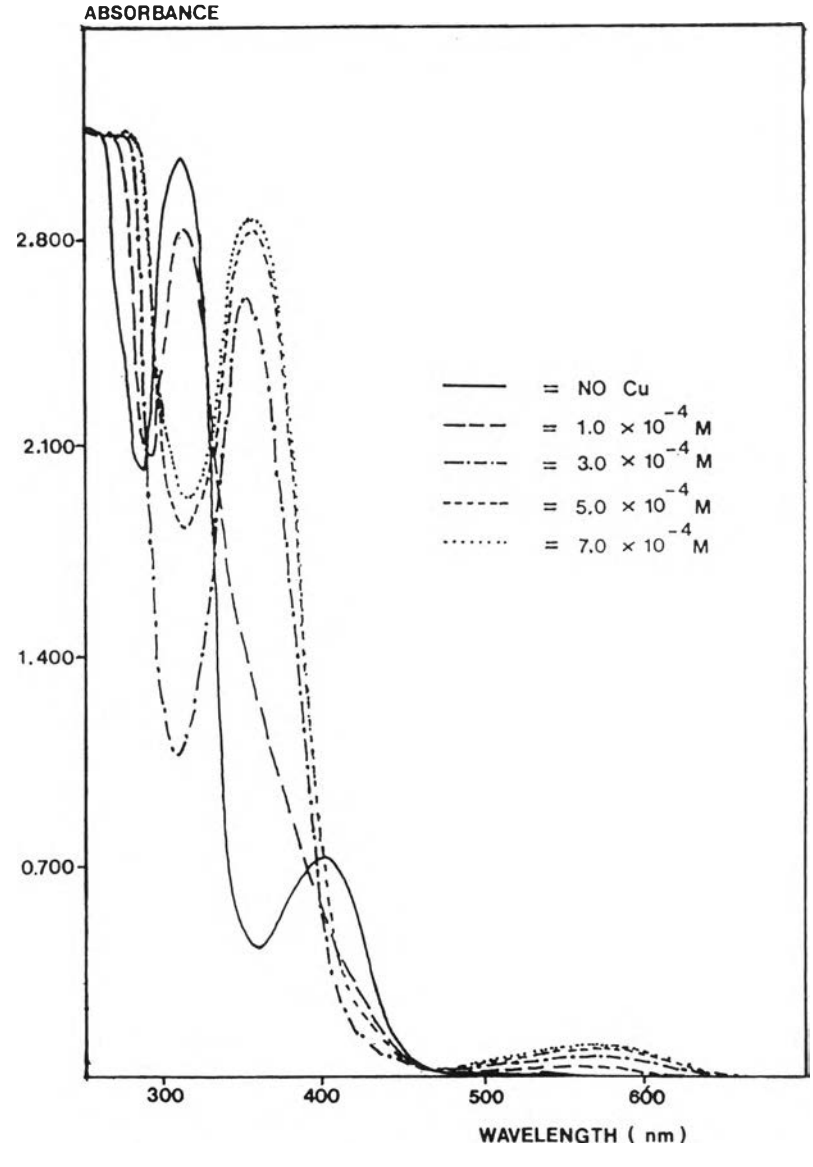

Fig 3.25 UV absorption spectra of Cu(II)-Salen complex in absolute methanol at constant Salen concentration (5.0×10^{-4} M)

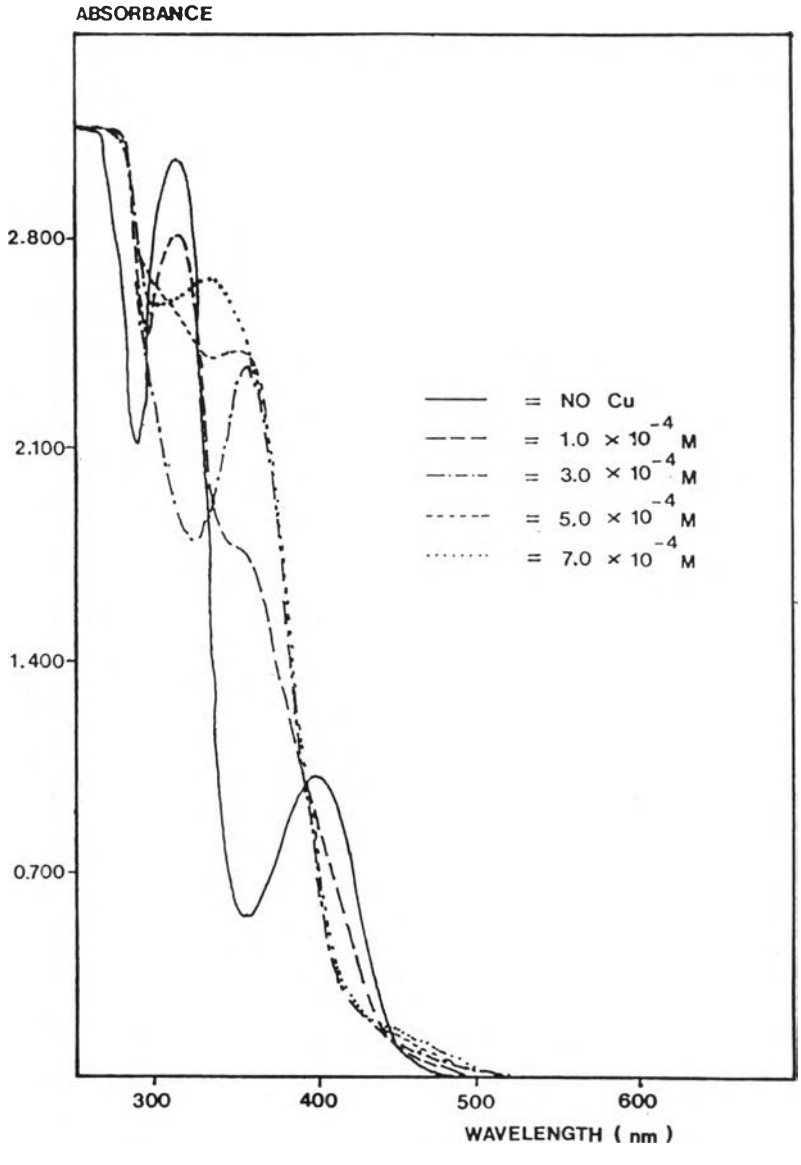

Fig 3.26 UV absorption spectra of Cu(II)-Saltn complex in absolute methanol at constant Saltn constant (5.0×10^{-4} M)

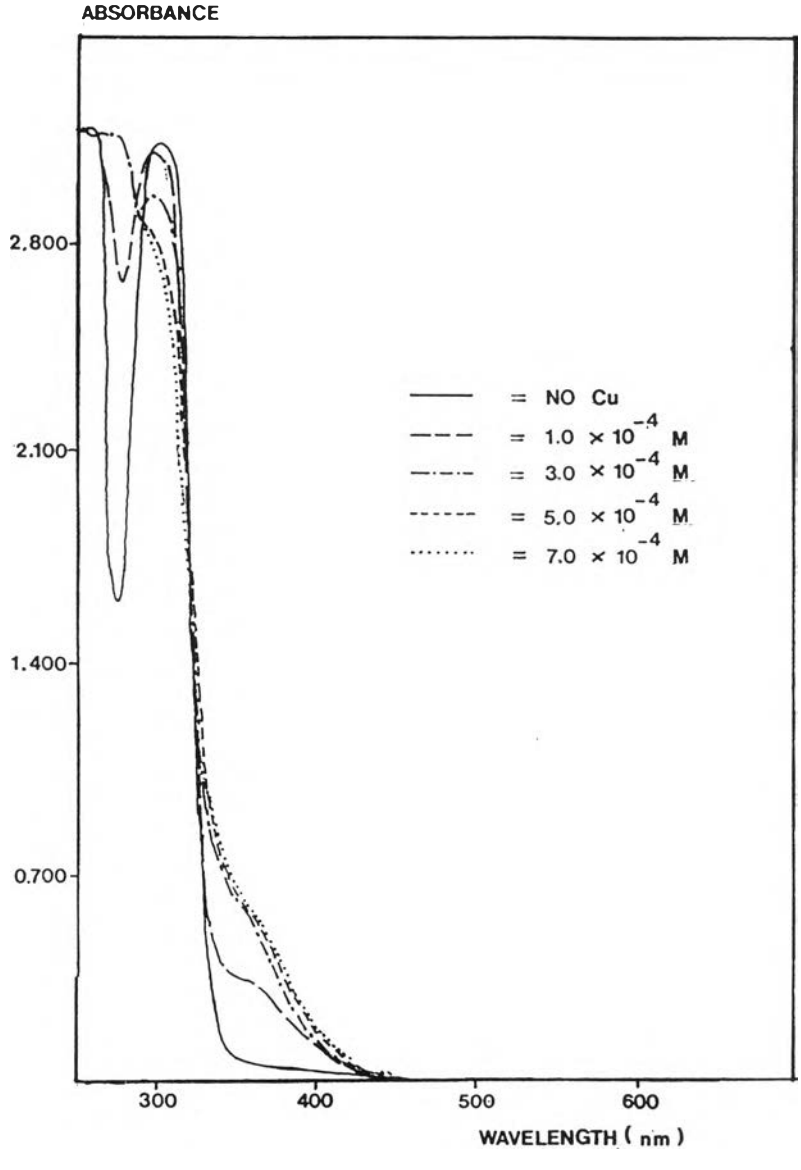

Fig 3.27 UV absorption spectra of Cu(II)-[O-en-N-tn] complex in absolute methanol at constant O-en-N-tn concentration (5.0×10^{-4} M)

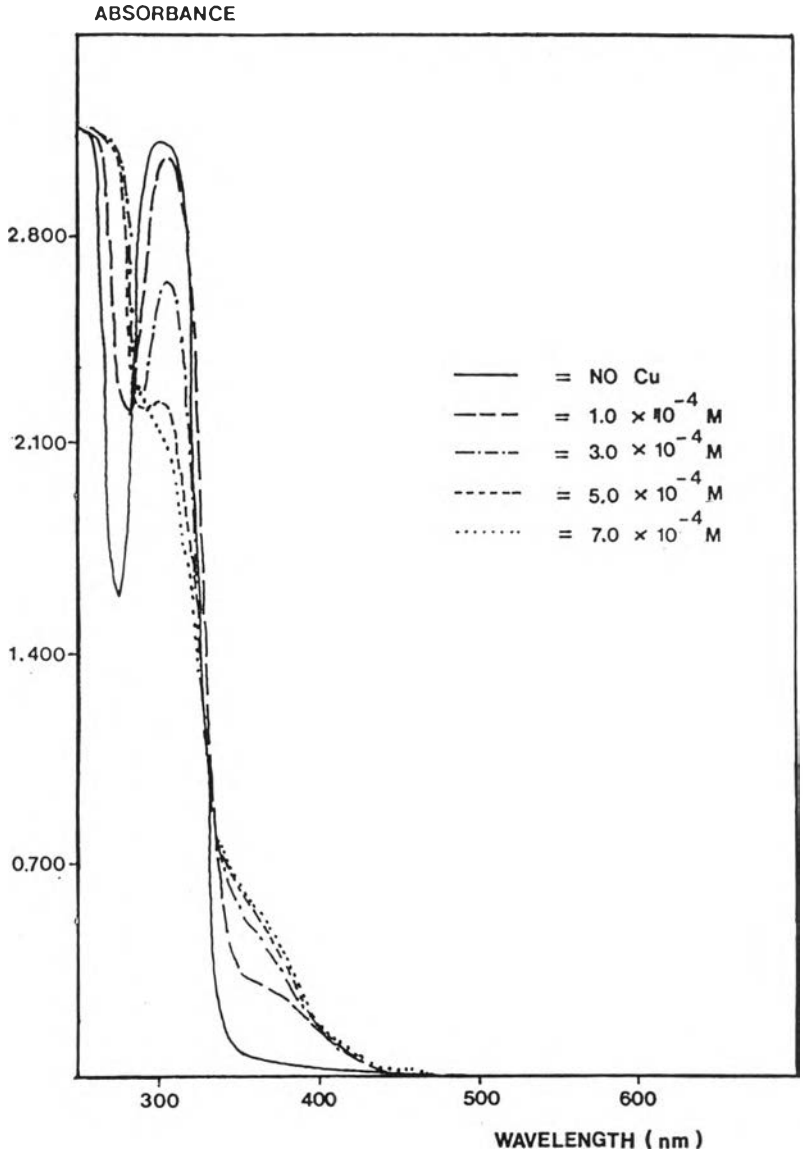

Fig 3.28 UV absorption spectra of Cu(II)-[O-tn-N-tn] complex in absolute methanol at constant O-tn-N-tn concentration (5.0×10^{-4} M)

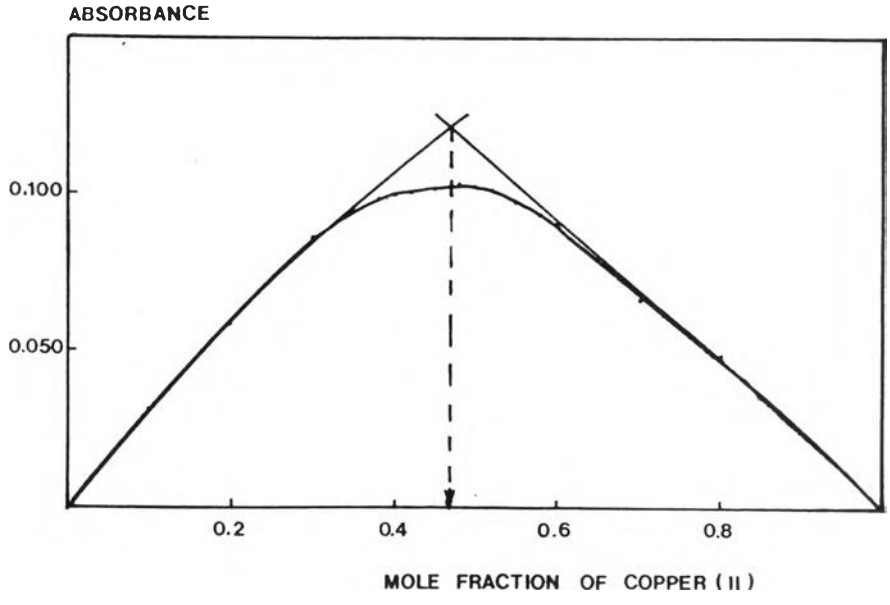

Fig 3.29 The Job's method plot of Cu(II)-Salen complex at 562 nm.

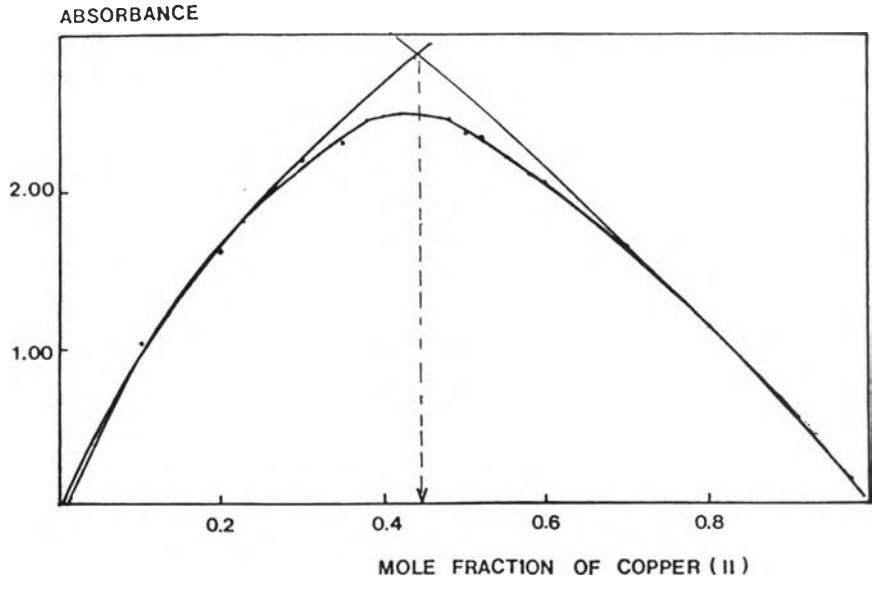

Fig 3.30 The Job's method plot of Cu(II)-Saltn complex at 356 nm.

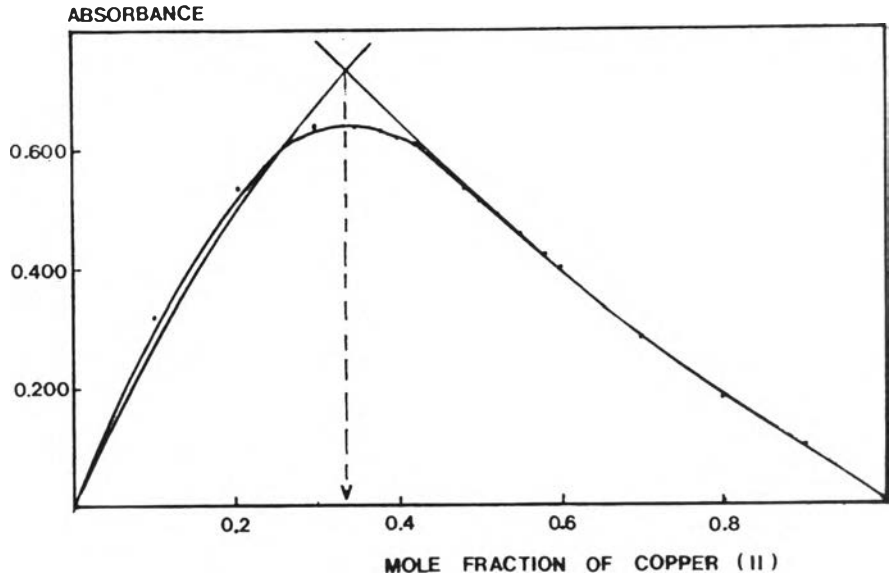

Fig 3.31 The Job's method plot of Cu(II)-[O-en-N-tn] complex at 352 nm.

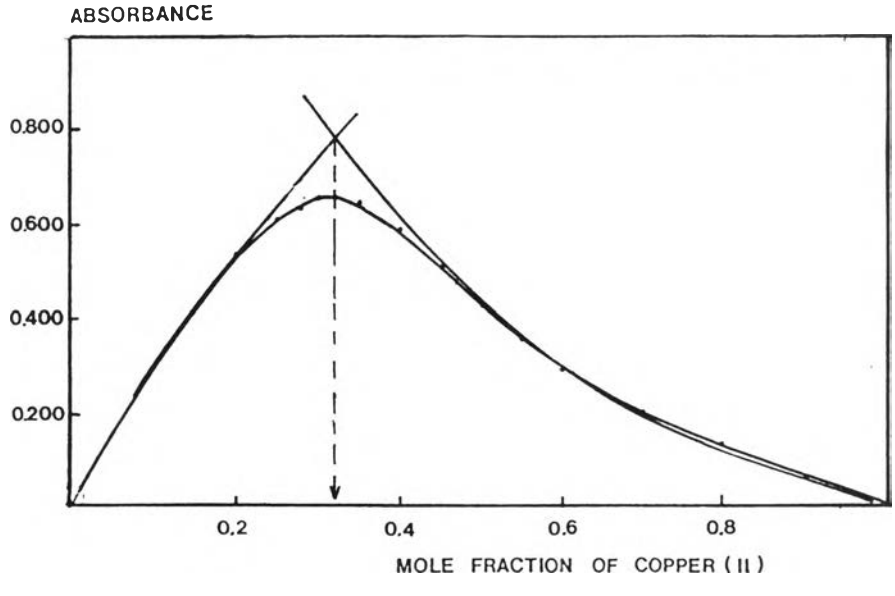

Fig 3.32 The Job's method plot of Cu(II)-[O-tn-N-tn] complex at 364 nm.

Table 3.8 The apparent stability constants of the copper -Schiff-base complexes[a].

Complex	Mole Ratio Metal : Ligand	log K[b]
Cu- Salen	1:1	4.71
Cu- Saltn	1:1	4.45
Cu-[O-en-N-tn]	1:2	8.62
Cu-[O-tn-N-tn]	1:2	8.85

[a] Studied in absolute methanol

[b] Calculation, see Appendix B.

3.4 Possibility of Copper Determination Using Salen as Spectrometric Reagent

In this research work, Salen was selected as possible spectrometric reagent for copper determination due to spectral change after complex formation of Cu^{2+} with Salen was clearly observed in comparision with Salen alone.

Optimum conditions were carefully studied in order to obtain the highest sensitivity of the method. In this work, the absorption measurement was carried out at wavelenght 562 nm (Figure 3.33); optimum Salen concentration, 1.0×10^{-2} M (Figure 3.34); the time for shaking,55 mins. (Figure 3.35); shaking stroke 250 strokes/min(Figure 3.36) and standing time at least 6 hrs (Figure 3.37). The pH of the aqueous phase was maintained at 7.2.

In the step of working range study of Cu-Salen complex, Salen concentration was kept constant with increments of Cu concentration. The obtained absorbances at 562 nm were shown in table 3.9 and Figure 3.38. The calibration curve was being linear in the range of 0-55 ppm of Cu(II). Accuracy of this method was examined and measured in term of % error. The result was indicated in Table 3.13. Precision was examined in term of % RSD and also correlation coefficient(r=0.999) as shown in Table 3.12. The molar absorbtivity calculated from slope was 2.90 x

10^2 L $mol^{-1}cm^{-1}$ which was equivilent to the specific absorbtivity of 4.6 x 10^{-3} mL $g^{-1}cm^{-1}$ and the Sandell sensitivity of 0.2174 g cm^{-2} (calculation, see in Appendix D).

Precision was examined in term of the relative standard deviation (RSD) by meaning the absorbance of thirteen measurements at 12.00 ppm of Cu(II). The examination gave the RSD as 1.02 % as indicated in Table 3.12. and limit of detection was 0.4 ppm,at absorbance 0.002

3.4.1 Effect of Interfering Ions

In this study, Cd(II) and Mn(II) were selected as coexisting ions. Effect of interfering ions on the absorbance of Cu(II)-Salen, by varying mole ratio between Cu:coexisting ion from 50:1 to 1:50 , is illustrated in Table 3.11. It is found that the coexisting ions have no effect on absorbance of Cu(II)-Salen in this system.

3.4.2 Application of the Method to the Determination of Copper in Solder Ingot

The invented method was also applied to determine copper in solder ingot. The step of sample preparation was explained in section 2.3.5. The pH of the aqueous phase was adjusted to minimum value as possible (4.5) to eliminate precipitation problem while still could gave good